Doctoral Dissertation

Three-dimensional image analysis of migration patterns of mouse neural crest cells using new monoclonal antibody (4E9R)

February, 1997

By
Yukihiko Kubota

CONTENTS

CHAPTER I

Production of new monoclonal antibody (4E9R) which identifies mouse neural crest cells

INTRODUCTION

Neural crest cells emigrate from the dorsum of the neural tube, migrate ventrally and give rise to a variety of derivatives such as pigment cells, neurons and their supporting cells in the peripheral nervous system, and ectomesenchymal cells in the vertebrate embryo (Weston, 1970; Le Douarin, 1982; Hall, 1988). Neural crest development advances along a rostral-to-caudal sequence. It has been suggested that neural crest cells function as a vehicle of the positional information, transporting it from somatic (dorsal) portions to visceral (ventral) structures (Hunt et al., 1991). Thus, these cells play important roles in construction of the vertebrate body organization.
Laboratory mice are particularly useful materials for studies of neural crest development. First, many genetic mutations which affect migration and differentiation of neural crest cells have already been reported (Silvers, 1979; Morrison-Graham and Weston, 1989). Second, artificial mutations produced by gene targeting or transgenic methods are available in genetic studies of neural crest development (Tanaka et al., 1990; Saga et al., 1992; George et al., 1993; Guillemot et al., 1993; Baynash et al., 1994; Hosoda et al., 1994; Schuchardt et al., 1994). However, little has hitherto been known about ontogeny of mouse neural crest cells due to lack of simple methods for identifying these cells.

HNK-1 (NC-1; see Vincent and Thiery, 1984; Tucker et al., 1984), a monoclonal antibody which identifies neural crest cells in many vertebrate embryos (Rickmann et al., 1985; Bronner-Fraser, 1986; Erickson et al., 1989; Sadaghiani and Vielkind, 1990; Hou and Takeuchi, 1994), has been used in experiments for analyzing migration patterns of these cells. However, HNK-1 does not recognize mouse neural crest cells. Molecules which specifically express in mouse neural crest cells have remained to be unknown. Nichols (1981, 1986) devised the histochemical method using toluidine blue to find early

migratory neural crest cells at cephalic levels of mouse embryos. However, it is difficult to distinguish between neural crest cells in their advanced migratory stages and mesoderm-derived mesenchymal cells by this method. Methods for marking mouse neural crest cells have been used in analyses of migratory pathways of these cells (Chan and Tam, 1988; Serbedzija et al., 1990, 1992). These studies have contributed to elucidating the migratory pathway of neural crest cells at a particular axial level. These cell-marking methods, however, contain some technical difficulties. In the present study, therefore, we attempted to prepare monoclonal antibodies which specifically recognize mouse neural crest cells in order to analyze their migration patterns using simple immunohistochemical methods.

MATERIALS AND METHODS

Production of hybridoma cells secreting rat anti-mouse monoclonal antibody (4E9R)

The mesencephalon and the first visceral arch were dissected from embryonic day (Ed) 8.5 (8-12 somite stages) and Ed 10.5 (35-39 somite stages) ddY mouse embryos (the day vaginal plugs were observed was defined as Ed 0), respectively. Their tissues were homogenized in Dulbecco's PBS (Nissui) and used as immunogens. These were immunized into the peritoneal cavity of young Wister rats or an Armenian hamster. The immunizations were performed five times, every two or three weeks. The immunogens were mixed with Freund's complete adjuvant (Difco Laboratories) on the first injection and with Freund's incomplete adjuvant (Difco Laboratories) from the second to the fourth injection. On the final injection, they were not mixed with the adjuvant. Three-days after the final immunization, spleen cells from the immunized rats or the hamster were fused with mouse myeloma (X63-Ag8-653) cells using 50% polyethylene glycol 4000 (Merck) in RPMI 1640 medium (Nissui). Fused cells were selected in S-clone medium (Sanko Junyaku) containing 100μM hypoxanthine, 0.4μM aminopterin and 16μM thymidine (HAT; Boehringer Mannheim). Screenings of 1037 colonies of hybridoma cells formed in HAT-containing medium were performed by immunohistochemistry using frozen sections of the mesencephalon and the first visceral arch, and 203 colonies producing antibodies were obtained. Hybridoma cells were repeatedly cloned in S-clone medium supplemented with 2% fetal bovine serum (Hyclone) by the limiting dilution and the clone producing 4E9R was isolated. The hybridoma cell line established was cultured in RPMI 1640 medium supplemented with 5% fetal bovine serum, 10mM sodium pyruvate (Wako) and 0.6% kanamycin sulfate (Wako). Immunoglobulin

subclass of 4E9R was determined by the isotyping kit for rat monoclonal antibodies (Serotec). The isotype was IgM (Fig. 1).

Primary cultures of mouse neural crest cells

Primary cultures of cranial neural crest cells were prepared using the mesencephalon of Ed 8.5 ddY embryo. Neural folds at mesencephalic levels were dissected and cut into small fragments. These fragments were explanted in 35-mm culture dishes coated with collagen (Celtrix). Primary cultures of trunk neural crest cells were exactly performed as described previously (Ito and Takeuchi, 1984; Ito et al., 1993). Dorsal trunk regions at last 6 somitic levels were dissected from Ed 9.5 (20 - 28 somite stages) ddY embryos. These regions were treated with 1% trypsin (1:250; Difco Laboratories) in Hanks' balanced salt solution (Nissui) containing 10mM Hepes (Sigma) for 20 min on ice. Trypsinization was terminated by replacing the enzyme with culture medium, and the tissue was then gently pipetted with a small pore Pasteur pipette to separate the neural tube from other components of the trunk. Neural tubes isolated were explanted into 35-mm culture dishes. Epithelial components in primary explants were mechanically removed with a tungsten needle after 48 hr in culture, leaving emigrated cephalic or trunk neural crest cells. Culture medium consisted of 85% α-modified minimum essential medium (Sigma), 10% of a selected batch of fetal bovine serum (Hyclone), 5% extract of day-11 chick embryos, 16 nM 12-o-tetradecanoylphorbol-13-acetate (TPA; Sigma), 20 nM cholera toxin (Sigma), and 50 μg/ml gentamycin (Sigma). The culture medium was exchanged every other day. The cultures were incubated at 37℃ in a humidified atmosphere containing 5% CO_2.

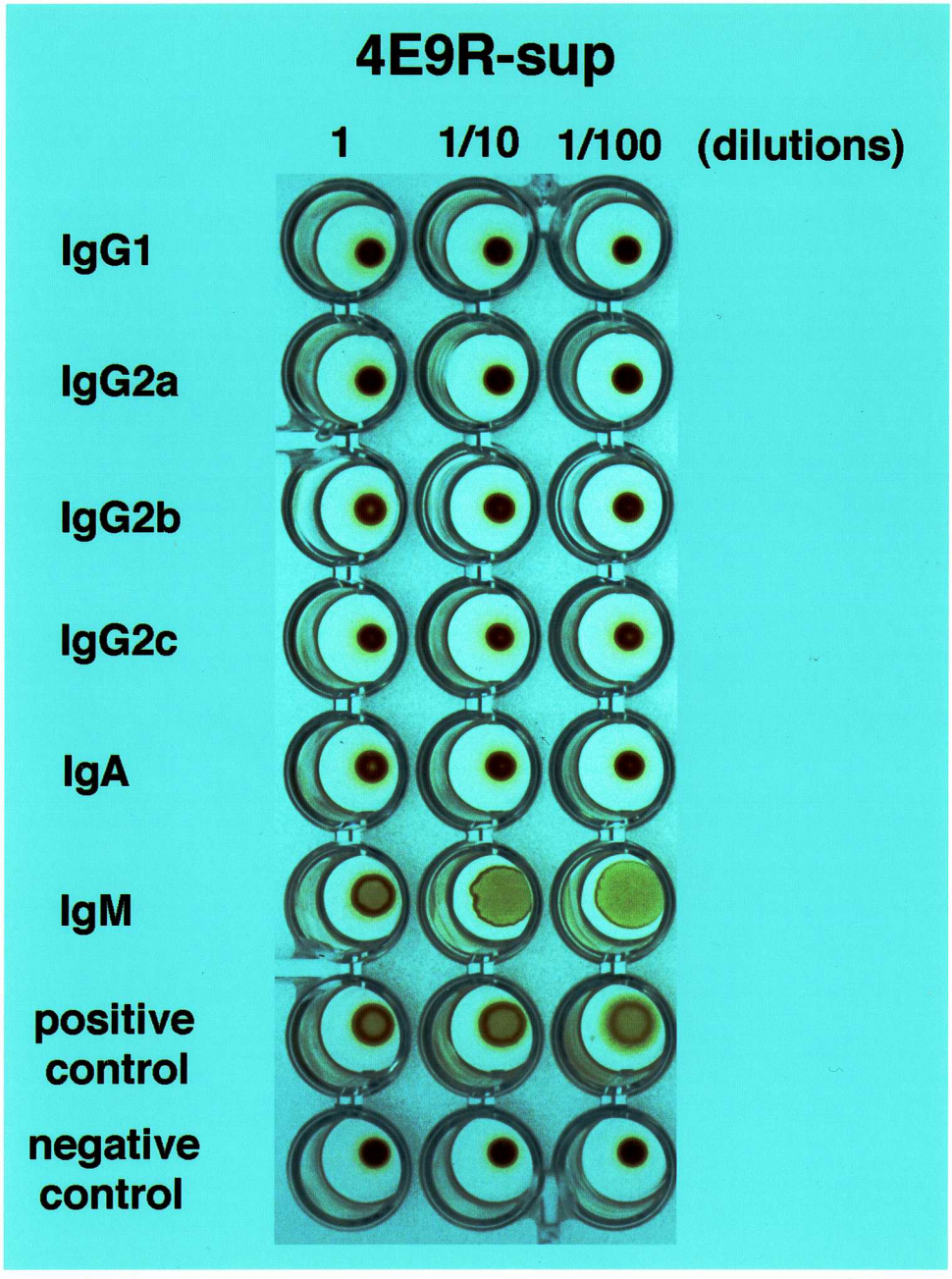

Fig. 1. Immunoglobulin subclass of 4E9R. Positive wells display part or full carpets of agglutination and negative wells show small circles. The isotype of 4E9R is IgM.

Immunohistochemistry

ddY mouse embryos in developmental stages from Ed 8.5 to Ed 10.5 were fixed with methanol containing 0.1% formaldehyde (MFA) for 10-20 min at -20℃. These fixed embryos were immersed in graduated sucrose solutions from 10% to 30% and subsequently embedded in OCT compound (Miles). Cryostat sections were cut at 10-20 μm and mounted on slide glasses coated with poly-L-lysine (Sigma). Primary cultures of mouse neural crest cells were fixed with ice-cold MFA for 10 min. The frozen sections and the fixed cultures were incubated in undiluted culture medium of 4E9R-producing hybridoma (4E9R-sup) overnight at 4℃ and subsequently in affinity-purified, FITC-conjugated goat anti-rat immunoglobulins (American Qualex) diluted to 1: 40 for 1 hr at room temperature. After immunostainings, the cultures were treated with 1 μg/ml Hoechst 33258 (Sigma) for nuclear stains. In double-stainings with anti-vimentin and 4E9R, the sections or the cultures were incubated in 4E9R-sup for 12 hr at 4℃ and then in rabbit anti-vimentin antibodies (dilution 1: 50; Medac) for 12 hr at 4℃ or mouse monoclonal anti-vimentin antibodies (dilution 10 μg/ml; Boehringer Mannheim) for 1 hr at room temperature. The following secondary antibodies were used: FITC-conjugated goat anti-rat immunoglobulins and affinity-purified, rhodamine-conjugated goat anti-rabbit (dilution 1: 50; Cappel) or anti-mouse (dilution 1: 40; Chemicon) IgG. These antibodies were pooled and used for 1 hr at room temperature. No differences between polyclonal and monoclonal anti-vimentin antibodies were found in distributions of anti-vimentin-immunoreactive cells in mouse embryos. Since both polyclonal and monoclonal antibodies detect a single band of approximately 57 kD in Western blotting using Ed 10.5 whole-embryo lysates, they have little cross-reactivities to other molecules. To examine staining patterns in different concentrations of 4E9R or anti-vimentin antibodies, dilution or enrichment of these antibodies was performed. 4E9R was concentrated up to 10 times by means of ultrafree-C3 regenerated cellulose membrane

units (Millipore). However, the staining patterns unchanged within range of practical concentrations of these antibodies. Fluorescence was viewed with the fluorescent microscope (BH2-RFK; Olympus).

Colchicine and cytochalasin B treatments

Primary cultures of mouse neural crest cells were treated with colchicine or cytochalasin B at culture day (Cd) 2. Colchicine was used at 63 μM for 24 hr and cytochalasin B treatment was performed at 21 μM for 1 hr (Lendahl et al., 1990). After treatments with these drugs, the cultures were used in the following double-stains: (1) In colchicine treatment, double-stainings with 4E9R and mouse monoclonal anti-α-tubulin (Amersham) were performed. Anti-α-tubulin was diluted to 1: 500 and applied to the cultures for 1 hr at room temperature. FITC-conjugated goat anti-rat immunoglobulins and rhodamine-conjugated goat anti-mouse IgG were pooled and used for 1 hr at room temperature. (2) After cytochalasin B treatment, the cultures were double-stained with 4E9R and rhodamine-conjugated phalloidin (Molecular Probes). Rhodamine-conjugated phalloidin (0.16 μM) was used for 1 hr at room temperature. For this double-labeling, neural crest cells were cultured in glass chamber-slides (Nunc) coated with collagen and fixed with methanol (for 1 min at -20℃) and acetone (for 4 min at -20℃), because the staining intensity of rhodamine-conjugated phalloidin is decreased by extended methanol fixation. After immunostainings, nuclei were stained with Hoechst 33258.

Three-dimensional image analysis of intracellular distributions of 4E9R-antigens and vimentin

To analyze intracellular localizations of 4E9R-antigens and vimentin, we examined distributions of 4E9R-antigens and vimentin in Cd 2 primary cultures of mouse neural

crest cells. After double-stainings with 4E9R and anti-vimentin, neural crest cells were observed with Olympus confocal laser scanning microscope (LSM-GB). Three-dimensional images of intracellular distributions of 4E9R-antigens and vimentin were reconstructed from serial confocal optical sections, using image-analyzing software [NIH Image and Spyglass Dicer (Spyglass)]. Subsequently, distributions of 4E9R-antigens and vimentin were analyzed in slices of these reconstructed images with Spyglass Dicer.

RESULTS

Spatiotemporal distribution patterns of 4E9R-positive cells in mouse embryos

We have examined distributions of 4E9R-immunoreactive cells in mouse embryos of embryonic day (Ed) 8.5 to 10.5 when extensive migration of mouse neural crest cells occurs. In mesencephalic regions of Ed 8.5 embryos, mesenchymal cells close to neural folds were 4E9R-positive (Fig. 2A, B). After 12-24 hr in development (Ed 9.0-9.5), streams of 4E9R-immunoreactive cells extending from cranial neural tubes to maxillary processes (Fig. 2C, D) and to first visceral arches (Fig. 2E, F) were observed in lateral regions of embryos. Further, 4E9R-positive cells were seen in presumptive trigeminal ganglia (Fig. 3A, B) and appeared in mesenchymal cell populations around both optic (Fig. 3C) and otic vesicles (Fig. 3D).

At forelimb-bud levels of Ed 9.5-10.5 embryos, 4E9R-positive cells were found in medial and lateral portions of sclerotomes (Fig. 4A). These cells colonized in the surroundings of the dorsal aorta (Fig. 4A) and in presumptive dorsal root ganglia (Fig. 4B). Whereas few 4E9R-immunoreactive cells were found at hindlimb-bud levels of Ed 9.5 embryos, masses of 4E9R-positive cells were present in the dorsolateral space adjacent to the ridge of the neural tube 24 hr later in development (Ed 10.5; Fig. 5A). Further, these cells entered anterior halves of sclerotomes (Fig. 5B, C). Distributions of 4E9R-immunoreactive cells were different between the rostral and the caudal level within each anterior half. While many 4E9R-positive cells were observed in both medial and lateral portions of sclerotomes at their rostral levels (Fig. 5D, E), distributions of these cells had a tendency to be restricted in medial portions of sclerotomes at the caudal levels (Fig. 5F, G). 4E9R-immunoreactive cells were seen beneath the dorsal epidermis (Fig.

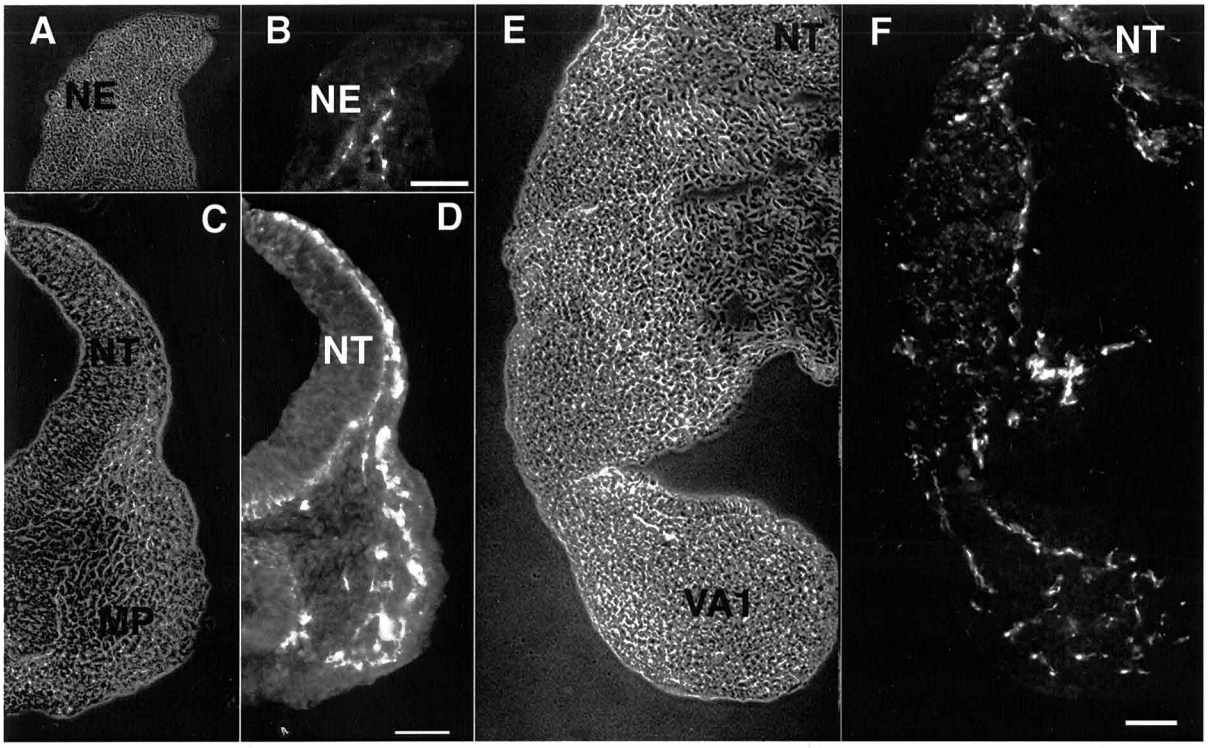

Fig. 2. Distributions of 4E9R-immunoreactive cells at cephalic levels. (**A**, **B**) Transverse section of the mesencephalic neural fold of Ed 8.5 embryo (**A**: phase contrast, **B**: immunofluorescent micrograph). 4E9R-positive cells are observed in mesenchymal cells close to the neural fold (**B**). (**C**, **D**) Transverse section at the maxillary process level of Ed 9.0 embryo (**C**: phase contrast, **D**: immunofluorescent micrograph). 4E9R-immunoreactive cells are found in the lateral region of the embryo (**D**). (**E**, **F**) Cross section at the first visceral arch level of Ed 9.5 embryo (**E**: phase contrast, **F**: immunofluorescent micrograph). Streams of 4E9R-positive cells extending from the cranial neural tube to the first visceral arch are observed in **F**. NE, neuroepithelium; NT, neural tube; MP, maxillary process; VA1, first visceral arch. Bars, 50 μm.

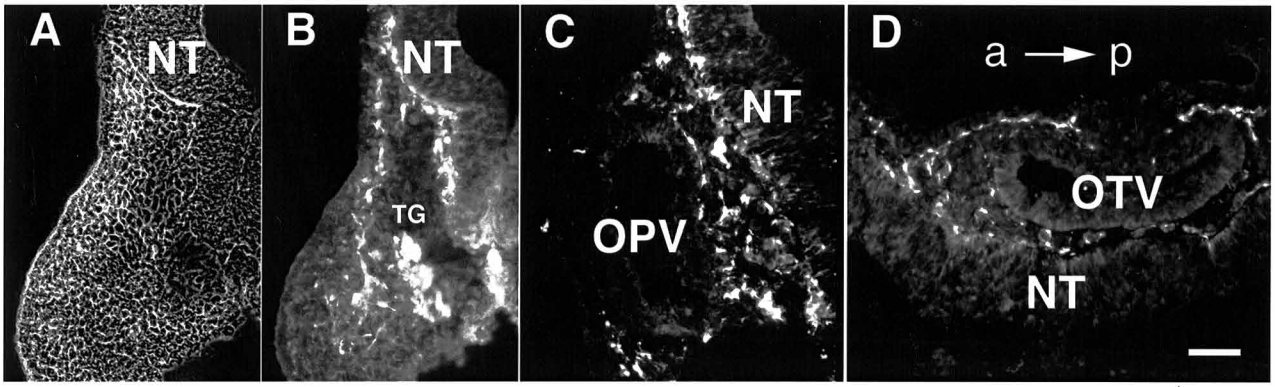

Fig. 3. 4E9R-immunoreactive cells in the trigeminal ganglionic region (**A**, **B**) and around the optic (**C**) and the otic (**D**) vesicle. (**A**, **B**) Transverse section at the first visceral arch level of Ed 9.0 embryo (**A**: phase contrast, **B**: immunofluorescent micrograph). (**C**) Cross section of the optic vesicle of Ed 9.5 embryo. (**D**) Coronal section of the otic vesicle of Ed 9.5 embryo. 4E9R-positive cells are observed in mesenchymal cell populations around both optic and otic vesicles. a and p show the anterior and the posterior side of the embryo, respectively. NT, neural tube; TG, presumptive trigeminal ganglion; OPV, optic vesicle; OTV, otic vesicle. Bar, 50 μm.

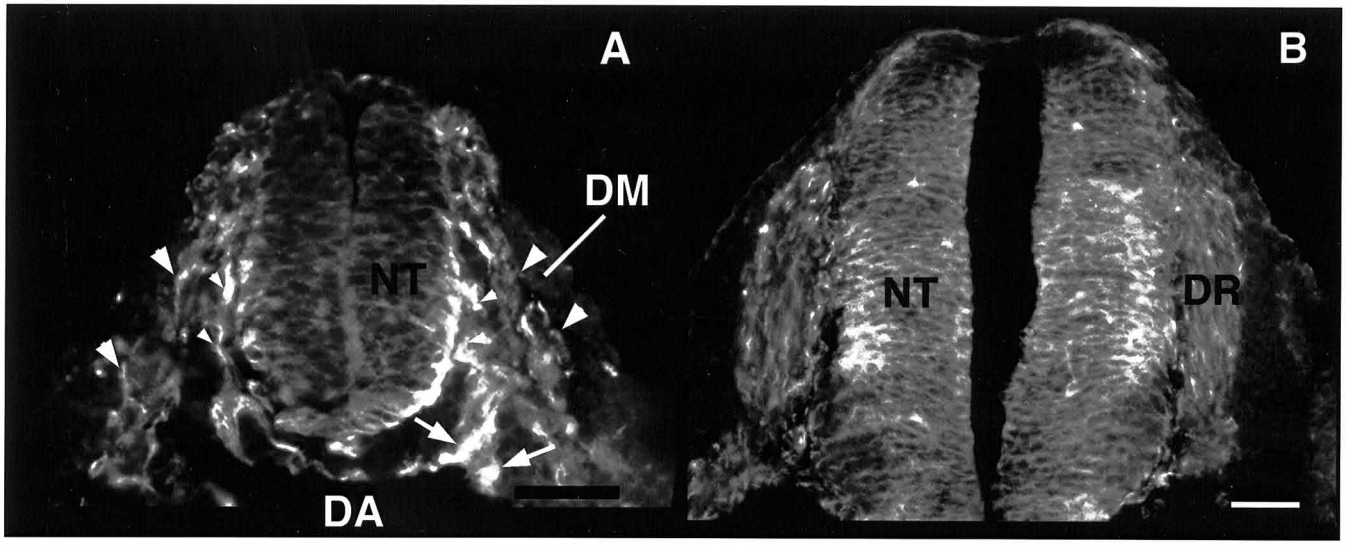

Fig. 4. Fluorescence micrographs of 4E9R-immunoreactive cells at forelimb-bud levels. (**A**) Transverse section at the forelimb-bud level of Ed 9.5 embryo. 4E9R-positive cells are observed in medial (small arrowheads) and lateral (large arrowheads) portions of sclerotomes and around the dorsal aorta (arrows). (**B**) Transverse section at the forelimb-bud level of Ed 10.5 embryo. Presumptive dorsal root ganglia (DR) are 4E9R-positive. DA, dorsal aorta; DM, dermamyotome; DR, dorsal root ganglia; NT, neural tube. Bars, 50 μm.

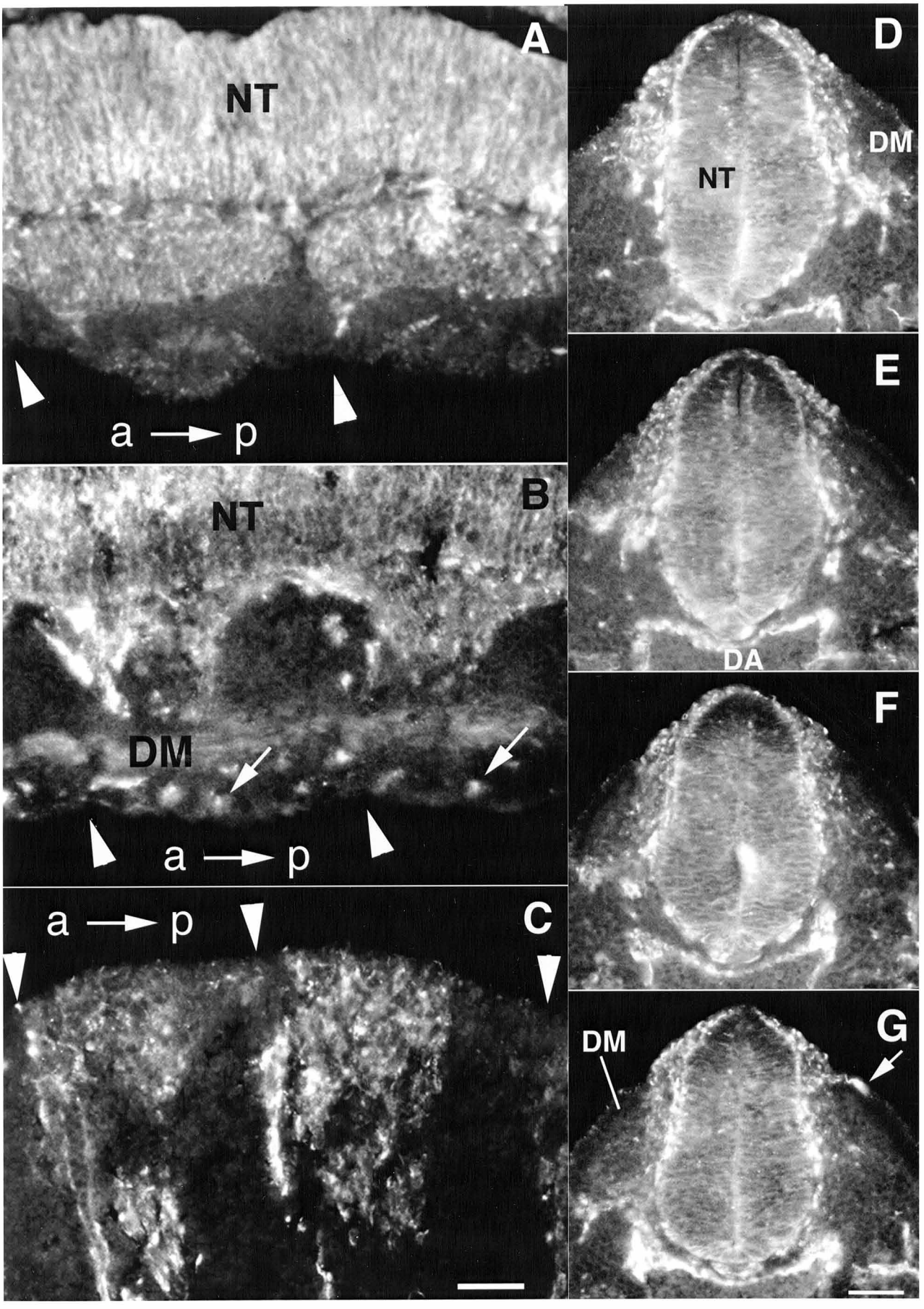

Fig. 5

Fig. 5. 4E9R-immunoreactive cells at hindlimb-bud levels of Ed 10.5 embryos. (**A**) Masses of 4E9R-positive cells are observed in the dorsolateral space adjacent to the ridge of the neural tube. (**B**) 4E9R-positive cells enter anterior halves of sclerotomes. **A** and **B** show horizontal sections of the same embryo. (**C**) Sagittal section. Note that distributions of 4E9R-positive cells are restricted to anterior halves of sclerotomes. (**D** - **G**) Serial transverse sections with 20μm thickness from the rostral (**D**) to the caudal (**G**) level within the anterior half of the sclerotome. One somite length along the anteroposterior axis at this stage is about 200 μm and distributions of 4E9R-positive cells were restricted in the dorsolateral space adjacent to the ridge of the neural tube in the section approximately 20 μm more rostral than **D**. **D**, **E** and **F**, **G** therefore show distributions of 4E9R-positive cells at the rostral and the caudal level within the anterior half of the sclerotome, respectively. 4E9R-immunoreactive cells are observed in medial and lateral portions of sclerotomes (**D**, **E**). Most 4E9R-positive cells are seen in medial portions of sclerotomes (**F**, **G**). 4E9R-immunoreactive cells are also found beneath the epidermis close to the dermamyotome (arrows in **B** and **G**). Arrowheads indicate somitic boundaries. a and p show the anterior and the posterior side of the embryo, respectively. NT, neural tube; DM, dermamyotome; DA, dorsal aorta. Bars, 50 μm.

この chapter が最初にならなかった理由は？

5B, G).

Intracellular localization of 4E9R-antigens in mouse neural crest cells

To confirm the presence of 4E9R-antigens in mouse neural crest cells and elucidate intracellular distributions of these antigens in these cells, their primary cultures were immunostained by 4E9R. In primary cultures of trunk neural crest cells, 76% of total cells were 4E9R-immunoreactive at culture day (Cd) 2 (Fig. 6A, B). The proportion of 4E9R-positive cells decreased accompanied with progress of the culture time and reached 36% at Cd 6 and 9% at Cd 12 (Table 1). In primary cultures of cranial neural crest cells, 82% of total cells were 4E9R-immunoreactive at Cd 2. However, the proportion of 4E9R-positive cells rapidly decreased and reached 14% at Cd 6 and 13% at Cd 12 (Table 1). Since it seems that 4E9R-antigens are localized on cytoskeletal components in mouse neural crest cells (Fig. 6A), colchicine or cytochalasin B treatment was performed to analyze intracellular sites of 4E9R-antigens in more detail (Fig. 6). When microtubules were disrupted by colchicine treatment (Fig. 6C), the intracellular distribution of 4E9R-positive filaments changed and an accumulation of 4E9R-antigens was observed in the surroundings of nucleus (Fig. 6E, G). The distribution of 4E9R-positive filaments was hardly affected by cytochalasin B treatment (Fig. 6F) despite abnormal changes in the cell and the nuclear morphology (Fig. 6H) through disorganization of microfilaments (Fig. 6D).

To compare intracellular distributions of 4E9R-antigens with those of vimentin in mouse neural crest cells, which is a typical intermediate filament in most mesenchymal cells including neural crest cells (Ziller et al., 1983; Cochard and Paulin, 1984; Erickson et al., 1987), we examined the distributions in mouse neural crest cells double-stained with 4E9R and anti-vimentin using the confocal laser scanning microscope (Fig. 7). The three-dimensional image of vimentin (Fig. 7C) reconstructed from optical sections

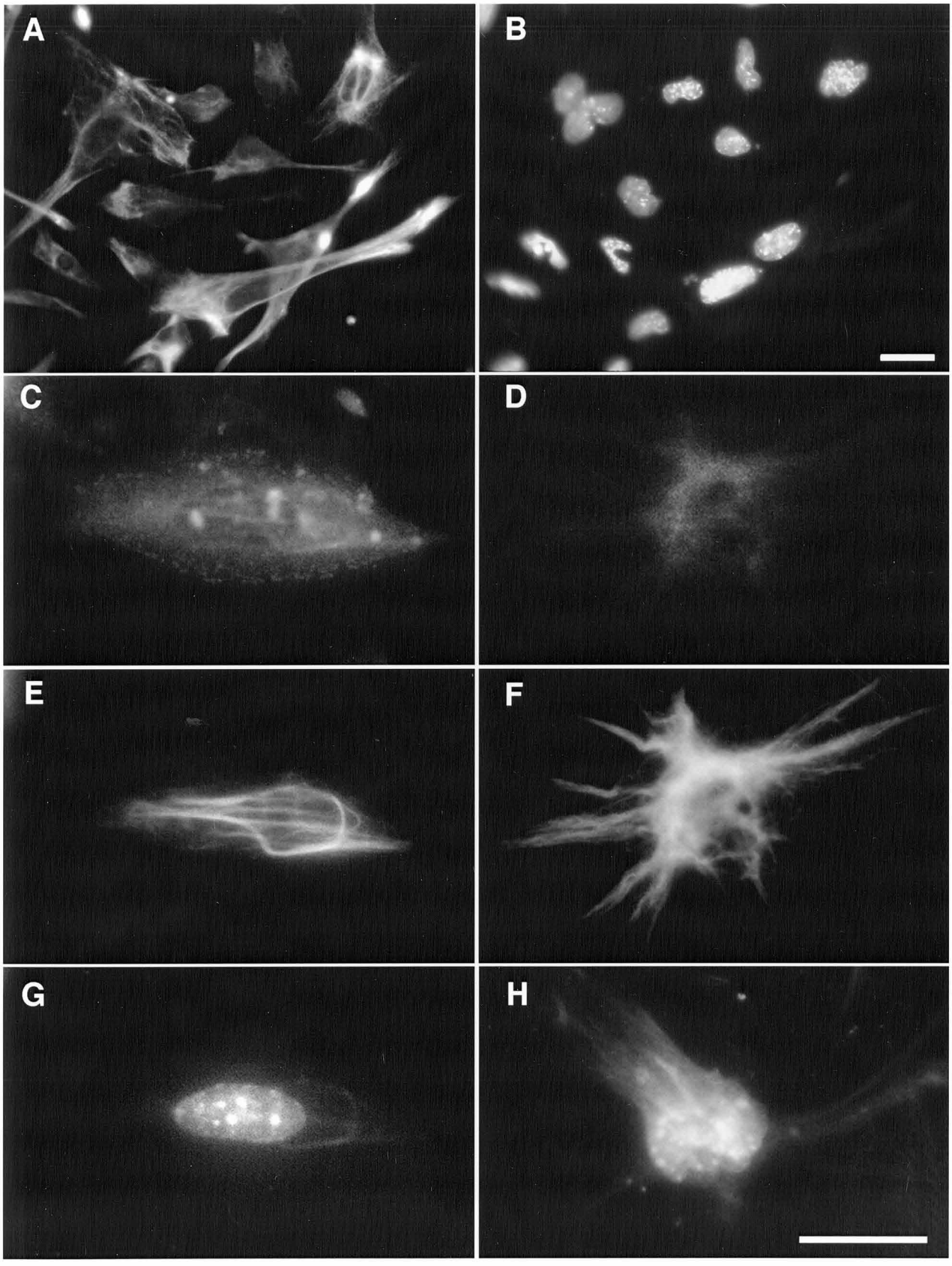

Fig. 6

Fig. 6. (**A**, **B**) Primary cultures of trunk neural crest cells at culture day (Cd) 2 . Most cells in the cultures are 4E9R-immunoreactive (**A**). **B** indicates nuclear stains in the same field as **A**. (**C** - **H**) Colchicine or cytochalasin B treatment of mesencephalic neural crest cells at Cd 2. The colchicine-treated cell triple-stained with anti-tubulin (**C**), 4E9R (**E**) and Hoechst (**G**). The cytochalasin B-treated cell triple-stained with rhodamine-conjugated phalloidin (**D**), 4E9R (**F**) and Hoechst (**H**). Bars, 25 μm.

Table 1. 4E9R-positive cells in cranial and trunk neural crest cell primary cultures

Culture day	Cranial neural crest cell	Trunk neural crest cell
2 days	1952/2384 (82%)[a]	3711/4903(76%)
6 days	236/1682 (14%)	2416/6772(36%)
12 days	267/2030 (13%)	492/5536(9%)

a) positive cells /total cells counted (%)

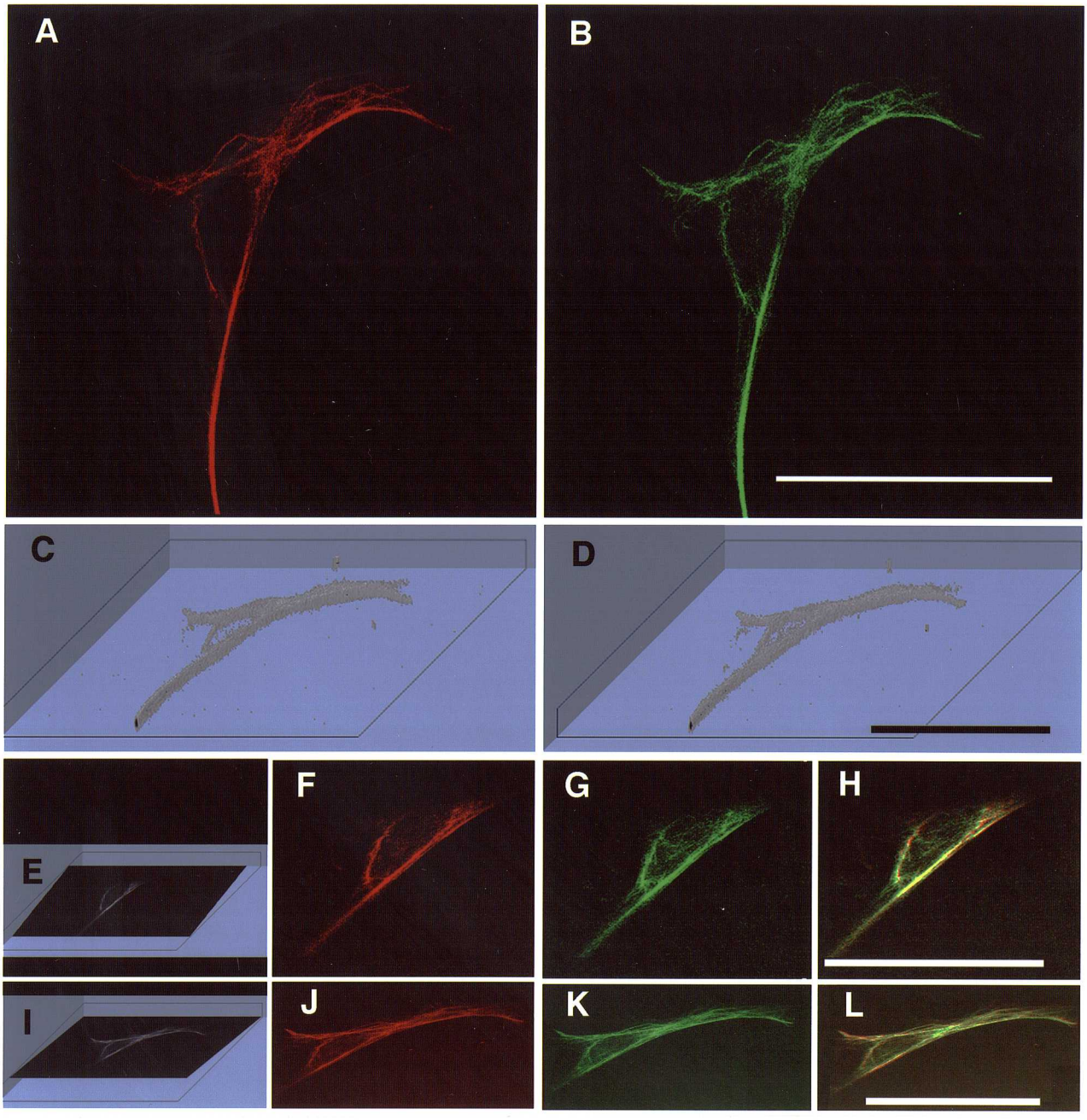

Fig. 7. Image analyses of intracellular distributions of 4E9R-antigens and vimentin in trunk neural crest cells double-stained with 4E9R and anti-vimentin. (**A**, **B**) Confocal images of distributions of vimentin (**A**) and 4E9R-antigens (**B**) in the same cell. (**C**, **D**) Three-dimensional reconstructions of vimentin (**C**) and 4E9R-antigens (**D**). Distributions of vimentin (**F**, **J**) and 4E9R-antigens (**G**, **K**) in 2 types of oblique slices (**E**, **I**). **F**, **G** and **J**, **K** show their distributions in slices cut at the same angles from the three-dimensional images. **H** and **L** display combined distributions of vimentin and 4E9R-antigens in the respective slices. Bars, 50 μm.

was identical with that of 4E9R-antigens (Fig. 7D). In slices of the respective three-dimensional images, distribution patterns of 4E9R-antigens were comparable with those of vimentin (Fig. 7E - L).

Distributions of 4E9R-positive cells and vimentin-containing cells in mouse embryos

Since 4E9R-antigens are likely to be closely related to vimentin in mouse neural crest cells, distributions of 4E9R-immunoreactive cells in Ed 8.5-10.5 embryos were compared with those of cells containing vimentin. Whereas almost all mesenchymal cells contained vimentin in Ed 8.5-10.5 embryos, more restricted cell-types were 4E9R-positive (Table 2). In Ed 8.5-10.5 embryos, 4E9R stained neuroepithelial cells, endothelial precursor cells derived from the primitive streak and endothelial cells in heart primordia and blood vessels (Table 2). The immunoreactivities of neural tubes (Fig. 4, 5) started to appear in ventral parts of these structures at cervical levels of Ed 9.0 embryos and rapidly extended to all axial levels.

Table 2. Distributions of 4E9R-immunoreactive and anti-vimentin-positive cells in mouse embryos

	4E9R			Vimentin		
	Ed8.5	Ed9.5	Ed10.5	Ed8.5	Ed9.5	Ed10.5[a]
(TRUNK)						
neural crest	++	++	++	++	++	++
limb mesenchyme	NA	+	+	NA	++	++
lateral plate	-	?	?	++	++	++
somite	-	NA	NA	+	NA	NA
dermamyotome	NA	-	-	NA	+	+
sclerotome	NA	-	-	NA	+	++
endothelium[b]	++	++	++	++	++	++
neural tube	-	+	+	-	+	++
(HEAD)						
neural crest	++	++	++	++	++	++
mandibular arch mesenchyme[c]	NA	+	+	NA	++	++
maxillary process mesenchyme[c]	NA	+	+	NA	++	++
cranial mesoderm	-	-	?	+	++	++
neural tube	-	-	+	-	+	++

a) Ed: embryonic day.
b) Endothelial precursors derived from the primitive streak and endothelial cells in heart primordia and blood vessels.
c) Most of mesenchymal cells are derived from neural crest cells.
++: positive(strong), +: positive, -: negative, NA: not applicable, ?: unclear.

DISCUSSION

4E9R identifies mouse neural crest cells

In the present study, distributions of 4E9R-immunoreactive cells were examined in migratory stages of mouse neural crest cells. In cephalic regions, 4E9R-positive cells were observed in mesenchymal cell populations close to neural folds of Ed 8.5 embryos. Twelve to twenty-four hours later, streams of 4E9R-positive cells extending from cranial neural tubes to maxillary processes and to first visceral arches were found in lateral regions of embryos. These observations are similar to the results obtained in studies of migratory pathways of mouse cranial neural crest cells with histochemical (Nichols, 1981, 1986) or cell-marking (Chan and Tam, 1988; Serbedzija et al., 1992; Osumi-Yamashita et al., 1994) techniques. 4E9R-immunoreactive cells, furthermore, colonized in presumptive trigeminal ganglia and peri-optic and peri-otic mesenchyme as mentioned previously in the mouse (Chan and Tam, 1988; Serbedzija et al., 1992; Osumi-Yamashita et al., 1994) and the rat (Tan and Morriss-Kay, 1986). At forelimb-bud and hindlimb-bud levels of Ed 9.5-10.5 embryos, 4E9R-positive cells entered anterior halves of sclerotomes and migrated along " ventrolateral pathways" (Loring and Erickson, 1987; Serbedzija et al., 1990; Tosney et al., 1994) in lateral portions of sclerotomes and/or along "ventromedial pathways" (Serbedzija et al., 1990) in medial portions of sclerotomes. These cells colonized in presumptive dorsal root ganglia and around the dorsal aorta, the embryonic region where sympathetic ganglia are formed. The migration patterns and colonization of 4E9R-positive cells observed in this study are comparable with those of amniote neural crest cells detected with HNK-1 (Rickmann et al., 1985; Bronner-Fraser, 1986; Erickson et al., 1989; Hou and Takeuchi, 1994). It has been suggested that neural crest cells migrating along dorsolateral pathways may not be HNK-1-

immunoreactive (Erickson et al., 1989). On the other hand, 4E9R-positive cells were seen in the dorsolateral pathway beneath the epidermis. 4E9R might recognize melanocyte precursors in mouse embryos. These results indicate that 4E9R identifies mouse neural crest cells derived from both cephalic and trunk levels. In primary cultures of these cells, we have shown that most cells are 4E9R-immunoreactive at culture day 2 and that the number of 4E9R-positive cells decreases along with progress of the culture period. When most of mouse neural crest cells express various phenotypes in vitro (Ito and Takeuchi, 1984; Ito et al., 1993), many cells lose their immunoreactivities against 4E9R. Thus, 4E9R recognizes mouse neural crest cells in early stages of their development, probably before these cells express overt differentiation phenotypes.

We have found that distribution patterns of 4E9R-positive mouse neural crest cells may be different between rostral and caudal levels within anterior halves of sclerotomes. While both ventromedial and ventrolateral pathways of 4E9R-immunoreactive crest cells were observed at the rostral levels, ventromedial pathways were only seen at the caudal levels. Since it is considered that 4E9R identifies the majority of mouse neural crest cells in their early development, this observation suggests that migration patterns of mouse neural crest cells may be different between the rostral and the caudal level within the anterior part of the sclerotome. Serbedzija et al. (1990) have suggested that sympathetic ganglia are mainly formed by neural crest cells migrating along ventrolateral pathways at forelimb-bud levels of Ed 9.0-9.5 embryos. At forelimb-bud levels of Ed 9.5 embryos, we have found that 4E9R-positive mouse neural crest cells moving along ventromedial pathways as well as ventrolateral pathways colonize in the surroundings of the dorsal aorta (see Fig. 4A). Sympathetic ganglia might be derived from neural crest cells passing through the 2 types of routes. 4E9R also recognized neuroepithelial cells and endothelial (precursor) cells in embryonic stages examined. In most cases, however, these cells are distinguishable from neural crest cells by cell morphology and/or their localization sites within embryos (Pardanaud et al., 1987; Coffin and Poole, 1988;

Garcia-Martinez and Schoenwolf, 1993).

Antigens recognized by 4E9R are related to vimentin

We have shown that 4E9R-antigens are present in intermediate filaments. Neural crest cells and their derivatives contain intermediate filaments; vimentin, neurofilaments and desmin (Ziller et al., 1983; Cochard and Paulin, 1984; Erickson et al., 1987; Ito and Siber-Blum, 1991). However, neurofilaments and desmin differ from 4E9R-antigens in their expression patterns and their locations within embryos (Cochard and Paulin, 1984; Erickson et al., 1987). This suggests that 4E9R does not recognize antigens on neurofilaments and desmin. It is well known that vimentin is a typical intermediate filament in mesenchymal cells such as neural crest cells and mesodermal cells (Ziller et al., 1983; Cochard and Paulin, 1984; Erickson et al., 1987). We have also shown that most mesenchymal cells and neuroepithelial cells contain vimentin but types of cells containing 4E9R-antigens are more restricted. However, intracellular distributions of 4E9R-antigens were similar to those of vimentin in mouse neural crest cells. These results suggest two possibilities. (1) 4E9R recognizes antigens which have a modification specific to a few cell types including neural crest cells and are covalently linked to vimentin. It has been shown that intermediate filaments contain epitopes modified by phosphorylation (Chou et al., 1990) and/or glycosylation (Vidrich et al., 1982; Steinert and Roop, 1988). It is conceivable that some of these epitopes may be cell-type-specific. (2) 4E9R-antigens are present in factors closely associated with vimentin. Intermediate filaments have various associated factors (Ciment et al., 1986; Albers and Fuchs, 1992). It is possible that some vimentin-associated factors may be expressed in a few cell types only. Unfortunately, 4E9R-antigens were unstable in biochemical analyses including Western blotting. We therefore could not elucidate molecular characteristics of these antigens in more detail.

It has been reported that the expression of vimentin is related to epithelial-mesenchymal transition of cells (Franke et al., 1982; Erickson et al., 1987; Greenburg and Hay, 1988; Boyer et al., 1989). Mesenchymal transformation of neuroepithelial cells plays an important role in formation of neural crest cells. 4E9R-antigens are closely related to vimentin and they are expressed in mouse neural crest cells during their early developmental stages. It thus seems conceivable that 4E9R-antigens may play a role in formation of mouse neural crest cells. Taken together, the present data show that the use of 4E9R provides a simple method for the identification of mouse neural crest cells and that it is applicable to various types of experiments.

CHAPTER II

Three-dimensional image analysis of migration patterns of neural crest cells in the trunk of the mouse embryo

INTRODUCTION

In the trunk of the amniote embryo, neural crest cells migrate along two predominant pathways (Weston, 1963; Le Douarin, 1973; Erickson et al., 1989; Hou and Takeuchi, 1994) : (1) the dorsolateral pathway between the dermamyotome and the epidermis (Serbedzija et al., 1989, 1990; Kubota et al., 1996) and (2) the ventral pathway through the rostral half of each sclerotome (Rickmann et al., 1985; Bronner-Fraser, 1986; Kubota et al., 1996). Furthermore, two different types of ventral routes have been found in the rostral half, that is the ventromedial pathway along the medial portion of the sclerotome (Serbedzija et al., 1990; Kubota et al., 1996) and the ventrolateral pathway along the lateral portion of the sclerotome (Loring and Erickson, 1987; Serbedzija et al., 1990; Tosney et al., 1994; Kubota et al., 1996). It has been known that the peripheral nervous system in the vertebrate shows the systematically segmented pattern in the location (Keynes and Stern, 1984, 1988). Thus, migration of neural crest cells along their ventral routes, which are precursors of neurons and their supporting cells in the peripheral nervous system, might be spacially and temporally regulated even in the rostral half of the sclerotome to generate peripheral nerve cells and their supporting cells in defined locations. A possible approach to elucidate this regulation is to obtain and analyze the three-dimensional information of migration patterns of neural crest cells in the sclerotome. The data of neural crest cell migration in the mouse trunk are scanty even though a few studies have been previously performed in the initial phases (Erickson and Weston, 1983; Martins-Green and Erickson, 1986) and in the migratory stages (Serbedzija et al., 1990). Since we have been successful in the production of a monoclonal antibody (4E9R) which identifies mouse neural crest cells (see CHAPTER I; Kubota et al., 1996), it has become possible to investigate migration patterns of these cells in more detail. In the present study, therefore, we have examined dynamic patterns

of migration of mouse neural crest cells in the rostral half of the sclerotome by three-dimensional image analysis using a confocal laser scanning microscope and image-analyzing software.

Many studies about the roles of extracellular matrix molecules (ECM) in development of migratory pathways of neural crest cells have been performed using avian embryos (reviewed by Bronner-Fraser, 1993) and it has been revealed that these molecules are profoundly implicated in their development. Thus, spatiotemporal changes of distributions of ECM in migratory regions of mouse neural crest cells might be closely related to formation of their migration patterns. However, little has been known about the roles of ECM in the formation, in spite of a few reports of distributions of ECM in migratory stages of mouse neural crest cells (Sternberg and Kimber, 1986a, b). In this study, therefore, double- and triple-stainings using 4E9R and antibodies against ECM were performed to analyze the roles of ECM in formation of migration patterns of mouse neural crest cells. Tenascin is one of noteworthy ECM (Chiquet-Ehrismann et al., 1986). It has been controversial that how this molecule participates in migration of neural crest cells (Tan et al., 1987, 1991; Stern et al., 1989). Knockout-mutant mice of ECM including tenascin have been produced by the gene-targeting method (Saga et al., 1992; George et al., 1993). We attempted to clarify the roles of tenascin in migration of trunk neural crest cells using tenascin-knockout mouse embryos (Saga et al., 1992).

MATERIALS AND METHODS

Mice

ddY, C3H/HeN and C3H/HeN-TN$^-$/TN$^-$ mice were used. C3H/HeN-TN$^-$/TN$^-$ is a null mutant of tenascin-C gene, produced by the gene targeting (Saga et al., 1992). Embryos were staged by scoring the number of somites. Almost observations and analyses were performed at 8 somitic levels in forelimb-bud regions and at 23 somitic levels in hindlimb buds.

Immunohistochemistry

Immunostainings were performed as described in CHAPTER I (Kubota et al., 1996). Mouse embryos were fixed with methanol containing 0.1% formaldehyde for 10-20 min at -20℃, immersed in graduated sucrose solutions and subsequently embedded in OCT compound (Miles). Cryostat sections were serially cut at 10-20 μm and mounted on albumin-coated slideglasses. The following primary antibodies were used: (1) rat monoclonal antibody-4E9R, which identifies mouse neural crest cells (Kubota et al., 1996). (2) Rabbit anti-mouse laminin (anti-LN; Collaborative Research). (3) Rabbit anti-mouse fibronectin (anti-FN, Chemicon). (4) Rabbit anti-human melanoma tenascin-C (anti-TNp; Hasegawa et al., in press). (5) Rat monoclonal anti-human recombinant tenascin-C (anti-TNm; Koyama et al., 1996). (6) Mouse monoclonal antibodies against native chondroitin sulfate (CS-56; Seikagaku Corp.) (see Avnur and Geiger, 1984). Affinity-purified secondary antibodies were used as follows: (1) FITC-conjugated goat anti-rat immunoglobulins (American Qualex). (2) DTAF (dichlorotriazinyl amino)-conjugated goat anti-rat IgG (Chemicon). (3) Rhodamine-

conjugated goat anti-rabbit IgG and anti-mouse immunoglobulins (Cappel). (4) AMCA (7-amino-4-methylcoumarin-3-acetate)-conjugated goat anti-rabbit IgG (Vector). In double-stainings with 4E9R and anti-extracellular matrix molecules antibodies, stains of 4E9R have always preceded those of anti-extracellular matrices. In double-stainings with anti-TNm and anti-LN, anti-LN was used after anti-TNm stain. Triple-stainings were performed with combinations of 4E9R, CS-56 and anti-LN or anti-TNp. Antibodies were used at the following dilutions: 4E9R, undiluted culture medium of the hybridoma; anti-LN, 1:200; anti-FN, 1:500; anti-TNp, 1:1000; anti-TNm, 1:50; CS-56, 1:500; secondary antibodies, 1:20 - 1:100. Primary antibodies except CS-56 were applied to cryosections for 12 hr at 4℃. CS-56 was used for 30 min at room temperature. It was important in this study to check the dilution rate and the incubation time of CS-56. Since the low dilution and/or the long incubation resulted in the strong immunoreactivities in almost embryonic regions, it was difficult to find regional differences of distributions of chondroitin sulfate by immunohistochemical methods used. Through checks of various combinations of the dilution rate and the incubation time, we selected the condition for the CS-56 stain described above. Sections were treated with secondary antibodies for 1 hr at room temperature.

Three-dimensional image analysis

Cryosections immunostained were image-analyzed using the confocal laser scanning microscope (MRC-500; Bio-Rad) and image-analyzing software [NIH image and Spyglass Dicer (Spyglass)]. Serial optical sections with 2μm thickness were obtained by the laser microscope and stored in the computer system (Comos) attached to it. These optical sections were processed by NIH image and reconstructed as three-dimensional images covering one somite by the image stack using Spyglass Dicer. In some cases, these three-dimensional images were sliced in various directions with

Spyglass Dicer to analyze distributions of immunolabeled cells and/or materials in detail. Since it is difficult to determine the number of neural crest cells in their migratory routes, the semiquantitative method was used to estimate the number of them in ventrolateral pathways (see Fig. 4). Optical sections obtained from transverse cryosections immunostained with 4E9R and anti-LN were divided into 600 compartments in the range extending from the top of the neural tube to the bottom of the tube along the dorsoventral (vertical) axis and from the bottom of the tube to the epidermis along the proximodistal (horizontal) axis. Compartments containing both of 4E9R-positive neural crest cells and boundaries between sclerotomes and dermamyotomes were counted in all optical sections where ventrolateral pathways were observed. The results are expressed as percentage of them in total compartments containing the boundaries. This evaluation method reflects the massive changes in the number of neural crest cells in ventrolateral pathways.

RESULTS

Rostrocaudal differences in migration patterns of neural crest cells within the sclerotome

We have shown in CHAPTER I (Kubota et al., 1996) that 4E9R-positive mouse neural crest cells enter anterior halves of sclerotomes and migrate along ventromedial and ventrolateral pathways, and have suggested that the ventrolateral pathway appears in a more restricted region within the anterior half. To analyze regional differences in migration patterns of mouse neural crest cells in the sclerotome in more detail, we made three-dimensional reconstructions covering one somite of serial cryosections immunostained with 4E9R and examined distributions of neural crest cells in various slices of the reconstructed images at forelimb-bud (Fig. 1) and hindlimb-bud levels (Fig. 2). Three types of regions within the sclerotome, among which migration patterns of neural crest cells differed, were found along the anteroposterior axis at both axial levels. At the rostral level of the anterior half of the sclerotome, both ventromedial and ventrolateral pathways were observed (A-R region; Fig. 1A, Fig. 2A). The region, where the ventromedial route is only present (A-C region; Fig. 1B, Fig. 2B), caudally followed A-R region. No neural crest cells were seen in the posterior half of the sclerotome (Po region; Fig. 1C, Fig. 2C). These regional differences of migration patterns of neural crest cells in the sclerotome were confirmed in horizontal slices of the somite. While neural crest cells were observed in the dorsolateral space adjacent to the roof of the neural tube at all levels along the anteroposterior axis (Fig. 1D, G, Fig. 2D, G), A-R, A-C and Po were found within the sclerotome (Fig. 1E, F, H, I, Fig. 2E, F, H, I). In A-R region, neural crest cells migrating along the ventromedial pathway as well as the ventrolateral route reached the level of the sympathetic nerve plexus (Fig. 1A, E, F, H, I). Neural crest cells in A-

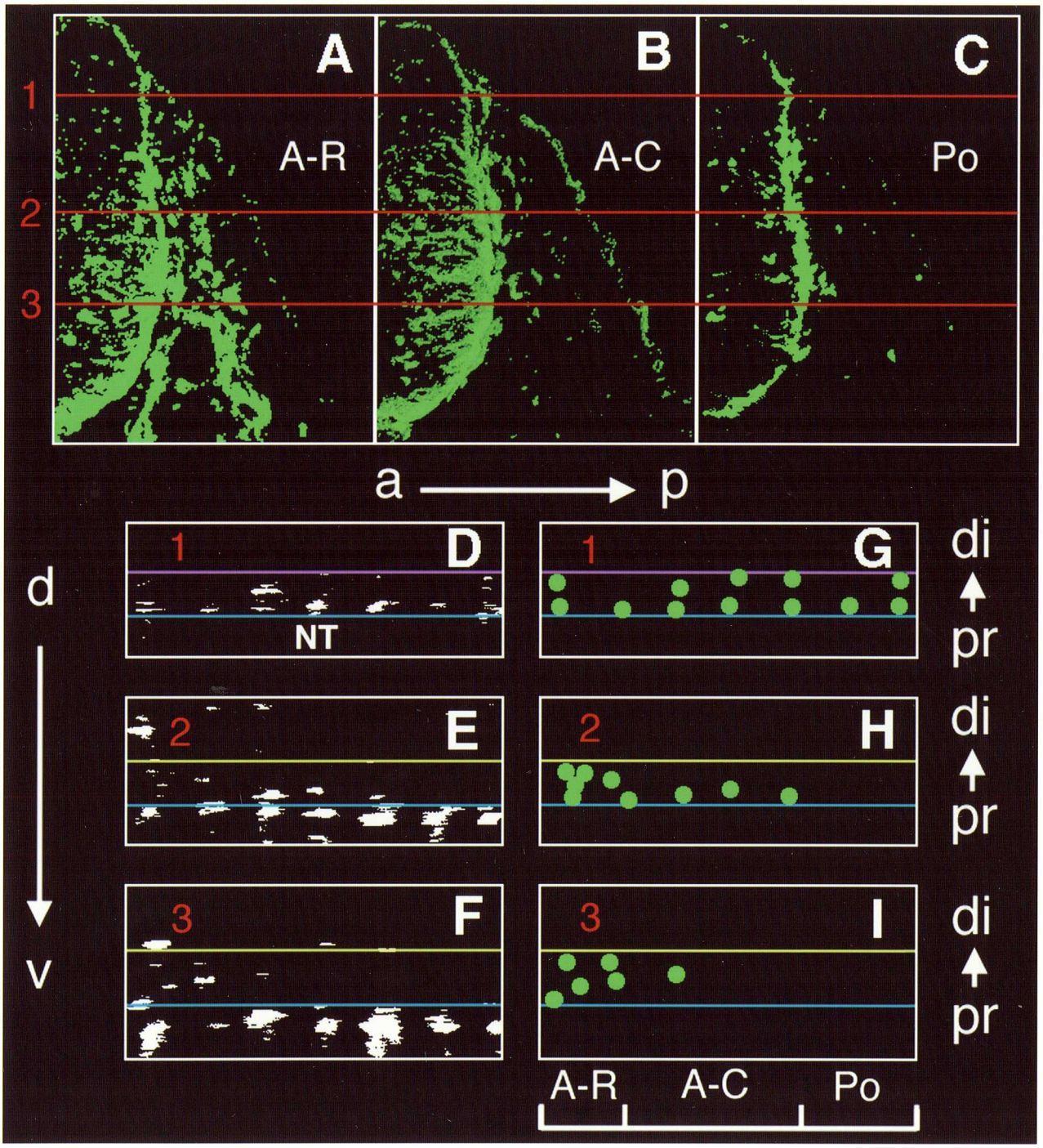

Fig. 1

Fig. 1. Three-dimensional image analyses of distributions of 4E9R-positive neural crest cells within the sclerotome at the 8 somitic (forelimb-bud) level of 24-somite ddY embryo. Optical sections produced by the confocal laser scannig microscope were processed at the same binary level (X=100) by NIH image. (**A** - **C**) Three images sliced transversely from a three-dimensionally reconstructed image covering one somite. Three regions having different migration patterns are present in the sclerotome, along the anteroposterior axis. Both of the ventromedial pathway along the medial portion of the sclerotome and the ventrolateral pathway along the border between the sclerotome and the dermamyotome are observed at the rostral level within the anterior half of the sclerotome, termed A-R region (**A**). The ventromedial pathway are only found at the caudal level within the anterior half of the sclerotome, termed A-C region (**B**). Neural crest cells are not present in the posterior half of the sclerotome (Po region; **C**). (**D** - **I**) Distributions of 4E9R signals in horizontal slices of the same reconstructed image. The reconstructed image was horizontally sliced at levels 1, 2 and 3 (red lines in **A**, **B** and **C**). Purple, yellow and blue lines show the epidermis, the boundary between the dermamyotome and the sclerotome and the border between the sclerotome and the neural tube, respectively. Crest-cell-specific 4E9R signals in **D**, **E** and **F** were schematically indicated as green dots in **G**, **H** and **I**, respectively. Neural crest cells are ubiquitously distributed in the dorsolateral space adjacent to the ridge of the neural tube (**D**, **G**). A-R, A-C and Po regions are observed within the sclerotome (**E**, **F**, **H**, **I**). Note that neural crest cells are absent in A-C region at level 3 (**B**, **F**, **I**). a, anterior; p, posterior; d, dorsal; v, ventral; pr, proximal; di, distal.

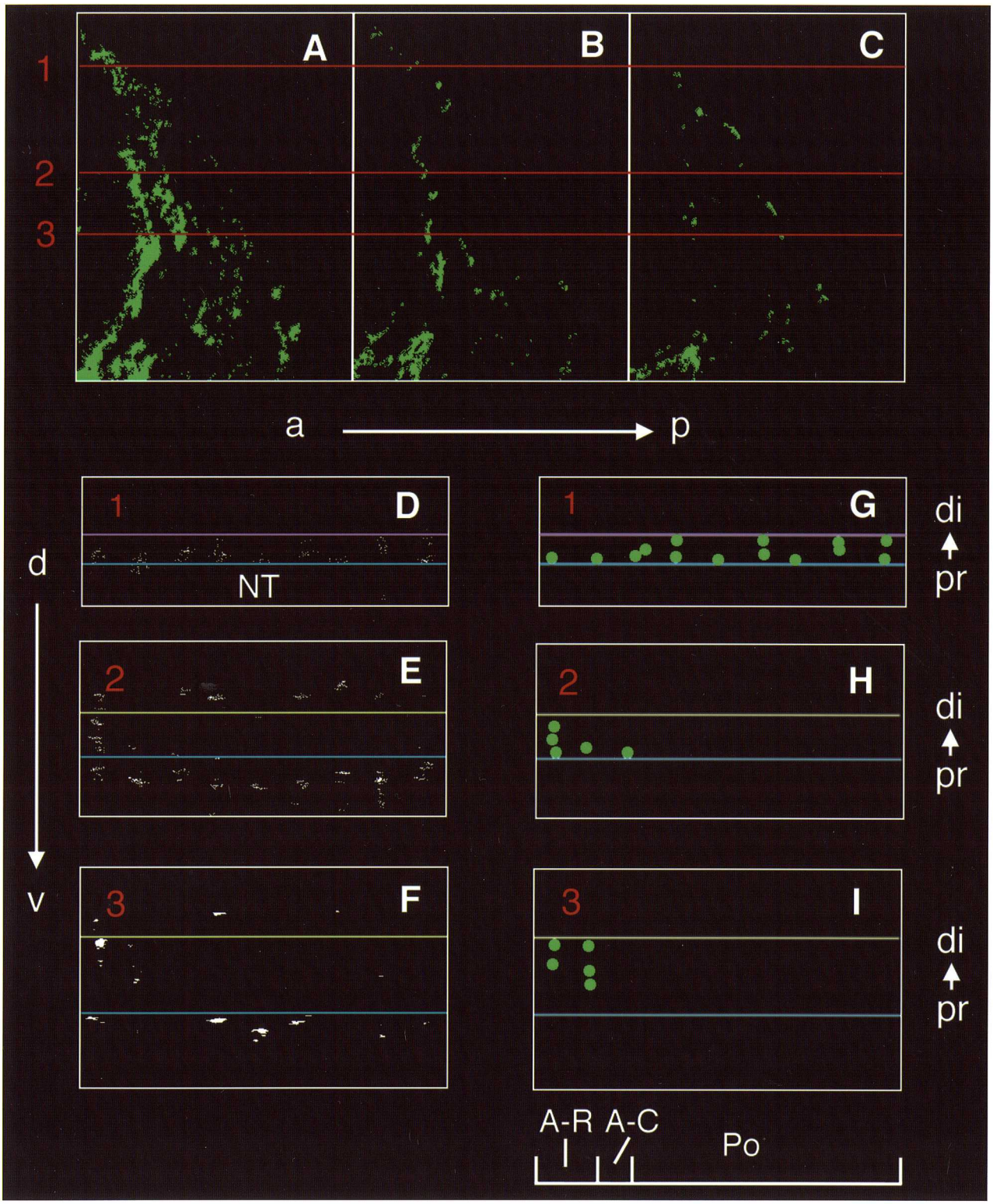

Fig. 2

Fig. 2. Three-dimensional image analyses of distributions of 4E9R-positive neural crest cells within the sclerotome at the 23 somitic (hindlimb-bud) level of 31-somite ddY embryo. Optical sections produced by the confocal laser scannig microscope were processed at the same binary level as **Fig. 1**. (**A** - **C**) Three images sliced transversely from a three-dimensionally reconstructed image covering one somite. A-R (**A**), A-C (**B**) and Po (**C**) regions are present in the sclerotome, along the anteroposterior axis. (**D** - **I**) Distributions of 4E9R signals in horizontal slices of the same reconstructed image. The reconstructed image was horizontally sliced at comparable levels 1, 2 and 3 (red lines in **A**, **B** and **C**) with **Fig. 1**. Purple, yellow and blue lines show the epidermis, the boundary between the dermamyotome and the sclerotome and the border between the sclerotome and the neural tube, respectively. Crest-cell-specific 4E9R signals in **D**, **E** and **F** were schematically indicated as green dots in **G**, **H** and **I**, respectively. Distribution patterns of neural crest cells in these horizontal slices are identical with those at forelimb-bud levels (**Fig. 1**). a, anterior; p, posterior; d, dorsal; v, ventral; pr, proximal; di, distal.

C region ceased their migration along the ventromedial pathway at the dorsal root ganglionic level (Fig. 1B, E, F, H, I, Fig. 2B, E, F, H, I). These rostrocaudal differences of migration patterns of neural crest cells within the sclerotome were similarly observed in all their migratory stages examined.

The rostrocaudal length of A-R, A-C or Po was measured during migratory stages of neural crest cells, based on the number of 2 μm-thick serial optical sections covering each region (Fig. 3). The length of every region changed as their migratory stages advanced. The proportion of A-R and Po in the sclerotome showed the maximum in early migratory stages (17 somite stages at forelimb-bud levels, 31 somite stages at hindlimb-bud levels). A-C increased along with development and occupied 60-70% of one-sclerotome length in late migratory stages (28 somite stages at forelimb-bud levels, 39 somite stages at hindlimb-bud levels). The decrease of A-R accompanied with the increase of A-C suggests changes of the number of neural crest cells in ventrolateral pathways in their migratory stages. These cells in the routes were semiquantitatively counted (Fig. 4). Analyses were performed in 4 areas consisting of dorsoanterior (DA), ventroanterior (VA), dorsoposterior (DP) and ventroposterior (VP) areas in the ventrolateral pathway. At forelimb-bud levels, the number of neural crest cells in all areas reached maximum in 24 somite stages (Fig. 4C) when the length of A-R became maximal (Fig. 3). In 28 somite stages, these cells more decreased in DA and DP (Fig. 4C). At hindlimb-bud levels, the number of neural crest cells migrating along ventrolateral pathways was smaller compared with forelimb-bud levels (Fig. 4D). Migratory stages when the number reached maximum were earlier in DA and DP (31 somite stages) than in VA and VP (37 somite stages; Fig. 4D).

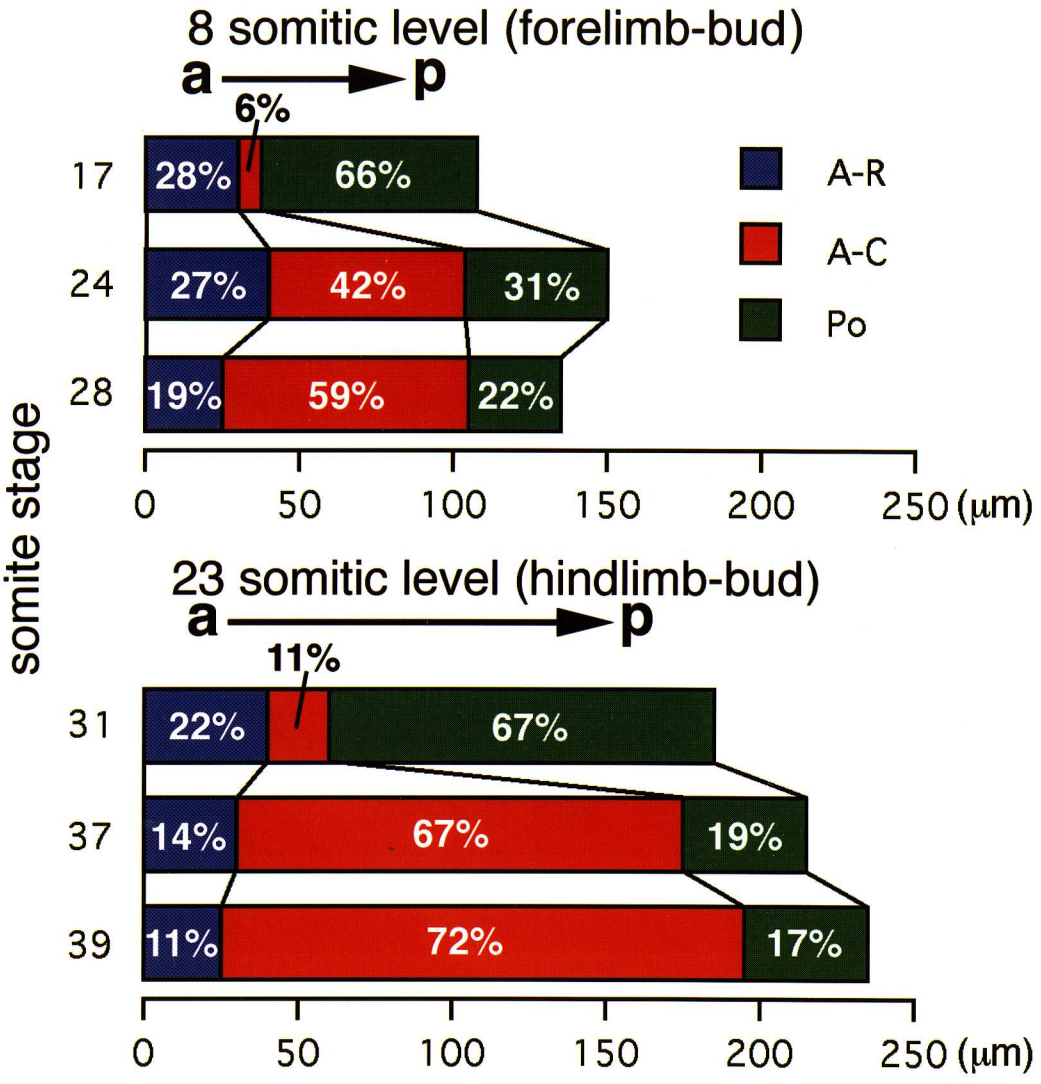

Fig. 3. Temporal changes of A-R, A-C and Po regions in migratory stages of neural crest cells in ddY embryos. Percentage of the rostrocaudal length of each region in the total sclerotome length is indicated in bars. Measurements were performed using 4 or 6 embryos. a and p show the anterior and the posterior side of the sclerotome.

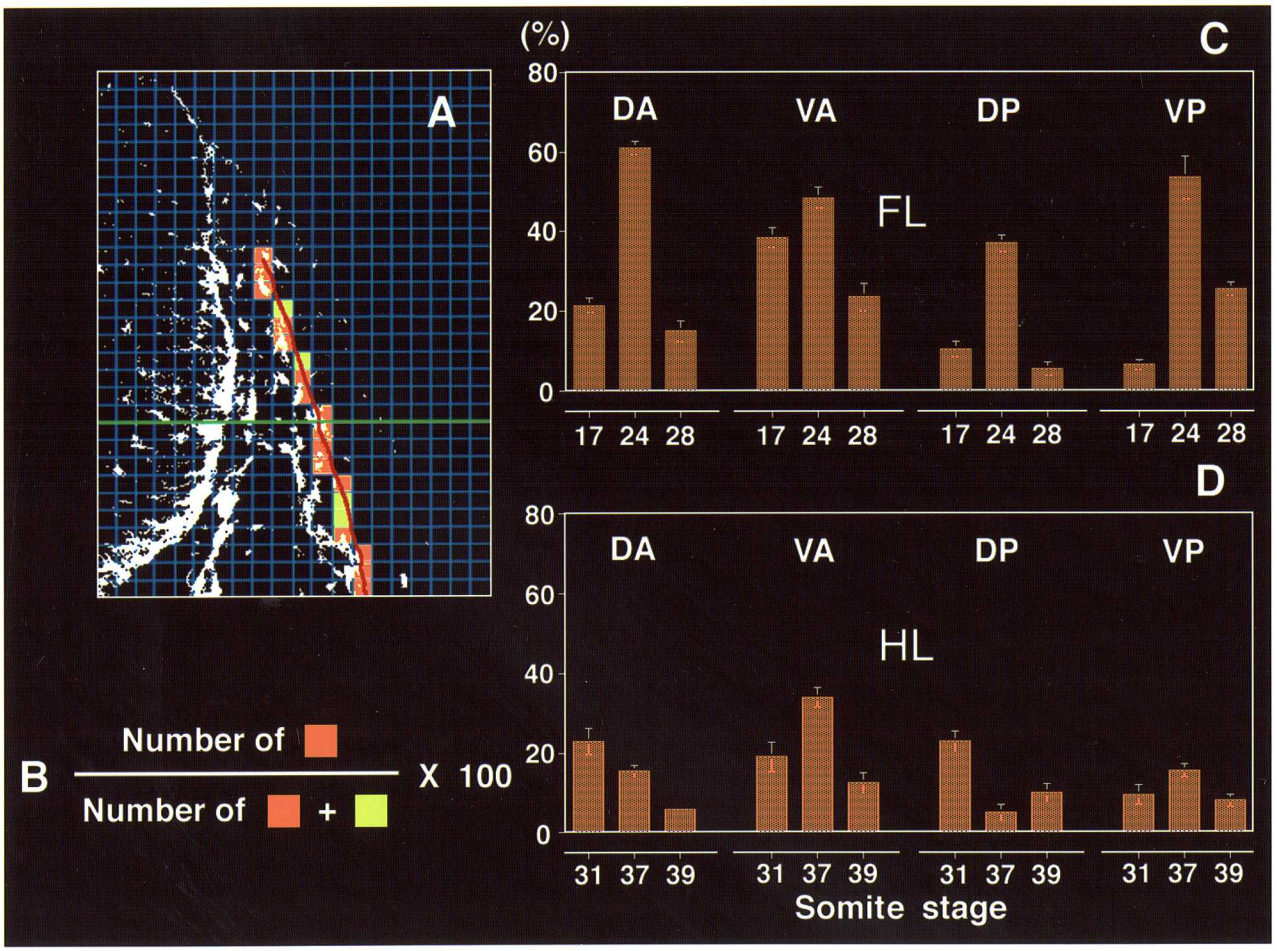
A
B
Number of
Number of +
X 100
(%)
C
80
60
40
20
0
DA
VA
DP
VP
FL
17 24 28
17 24 28
17 24 28
17 24 28
D
80
60
40
20
0
DA
VA
DP
VP
HL
31 37 39
31 37 39
31 37 39
31 37 39
Somite stage

Fig. 4

Fig. 4. Semiquantitative analyses of the number of neural crest cells migrating along ventrolateral pathways. (**A**) All transverse optical sections with 2μm thickness, where ventrolateral pathways were found, were divided into 20 (along the horizontal axis) X 30 (along the vertical axis) compartments (total 600). In early migratory stages of neural crest cells (17 somite stages at forelimb-bud levels or 31 somite stages at hindlimb-bud levels), boundaries between dermamyotomes and sclerotomes were determined by differences of cell morphology between sclerotomal and dermamyotomal cells. After 24 somite stages at forelimb-bud levels or 37 somite stages at hindlimb-bud levels, these boundaries were recognized by the presence of anti-laminin-positive basal lamina. Compartments containing the boundaries were regarded as major embryonic portions of ventrolateral pathways. Orange-colored compartments show those containing neural crest cells migrating along the ventrolateral pathway. Yellow compartments do not include neural crest cells. The results are expressed as percentage of the number of orange compartments in total number of compartments containing the boundary (total number of yellow and orange compartments) as shown in **B**. (**C**, **D**) Neural crest cells were counted in 4 areas divided equally along the dorsoventral and the anteroposterior axes, that is in DA (dorsoanterior), VA (ventroanterior), DP (dorsoposterior) and VP (ventroposterior). A green line in **A** shows the border between these areas along the dorsoventral axis (DA, DP and VA, VP). Bars represent the mean of the counting performed in 4 embryos. FL, forelimb-bud level; HL, hindlimb-bud level.

Distributions of extracellular matrix molecules in premigratory and migratory stages

To elucidate the roles of extracellular matrix molecules [fibronectin (FN), laminin (LN), chondroitin sulfate (CS), tenascin (TN)] in formation of migration patterns of mouse neural crest cells in the trunk, double- and triple-stainings using 4E9R and anti-extracellular matrix molecules antibodies were performed. Boundaries between dermamyotomes and sclerotomes did not contain LN in early migratory stages when ventrolateral pathways appeared in A-R regions (Fig. 5A). These boundaries became anti-LN-immunoreactive after middle migratory stages (24 somite stages at forelimb-bud levels, 37 somite stages at hindlimb-bud levels) at both forelimb-bud and hindlimb-bud levels (Fig. 5B-D). In all stages and axial levels examined, FN was uniformly distributed in sclerotomes (Fig. 5E-G). Differences of distributions of LN and FN were not detected in sclerotomes.

Before the invasion of neural crest cells into sclerotomes, CS initially appeared in cores of somites and subsequently the distributions shifted to anterior portions of sclerotomes (Fig. 6). This distribution of CS in the sclerotome was more evident in the dorsal portion (Fig. 6A). Distributions of CS in sclerotomes changed during migratory stages of neural crest cells. While clear signs of CS were not found at rostral levels of anterior halves of sclerotomes (A-R regions) in early to middle migratory stages (Fig. 7A), CS was distributed throughout A-C and Po (Fig. 7B, C). In A-C regions, however, CS was less in the surroundings of neural crest cells migrating along ventromedial pathways (Fig. 7B). CS-rich region anteriorly extended from the posterior side of A-R accompanied with advance of the migratory stage. This observation is comparable with the result that A-C expands along the anteroposterior axis (Fig. 3). In late migratory stages, the increase of CS content began to be observed in dorsal portions of A-R regions (Fig. 7D, H). Furthermore, an accumulation of neural crest cells appeared in the dorsal

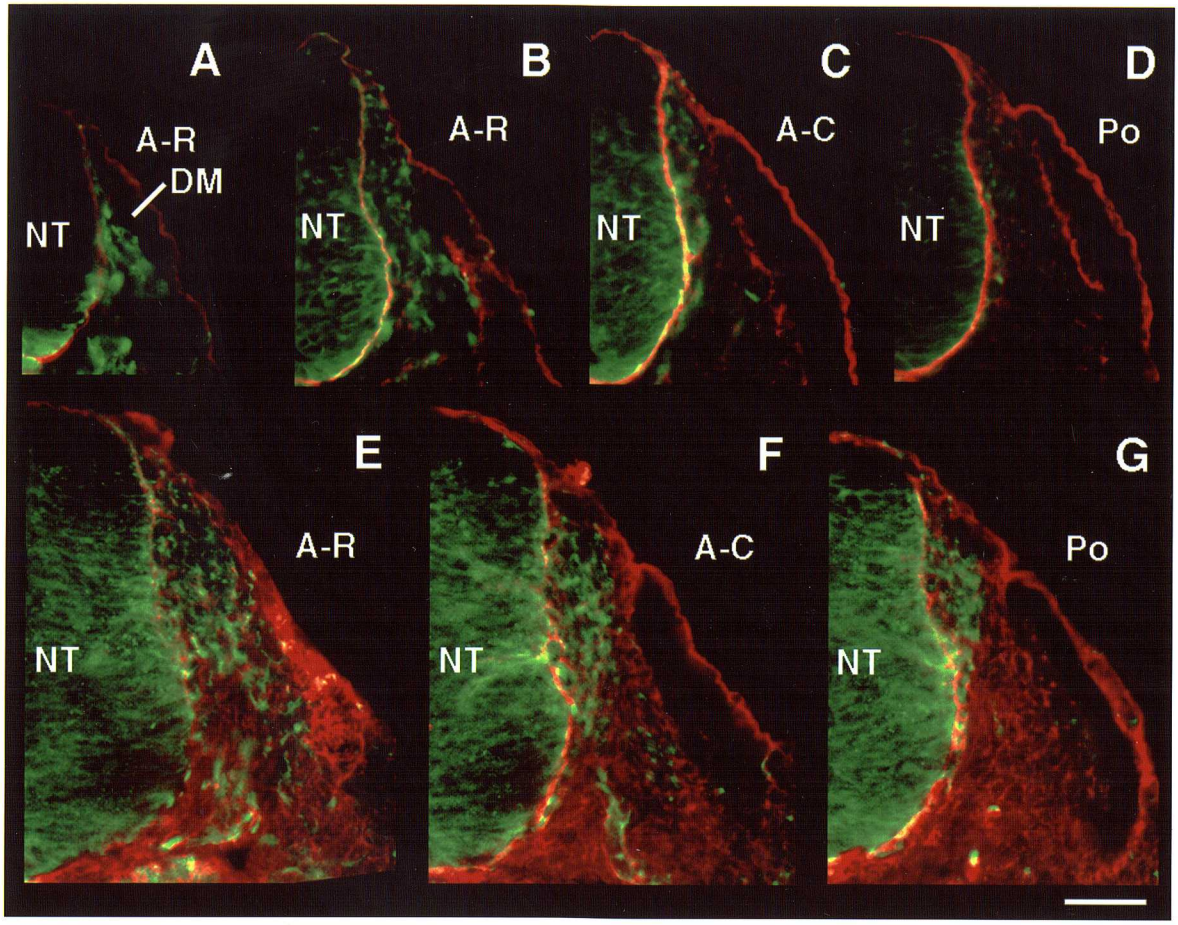

Fig. 5. (**A** - **D**) 4E9R-positive neural crest cells (green) and laminin (LN; red) in sections double-stained. (**A**) Transverse section of A-R region at the 8 somitic (forelimb-bud) level of 17-somite ddY embryo. Both ventromedial and ventrolateral pathways are observed. LN is not found in the boundary between the dermamyotome and the sclerotome. (**B** - **D**) Transverse sections of A-R (**B**), A-C (**C**) and Po (**D**) regions at the 8 somitic level of 24-somite ddY embryo. LN is found in the border between the dermamyotome and the sclerotome. (**E** - **G**) Fluorescence micrographs of neural crest cells (green) and fibronectin (FN; red). Transverse sections of A-R (**E**), A-C (**F**) and Po (**G**) regions at the 23 somitic (hindlimb-bud) level of 37-somite ddY embryo. FN is seen throughout the sclerotome. NT, neural tube; DM, dermamyotome. Bar: 50 μm.

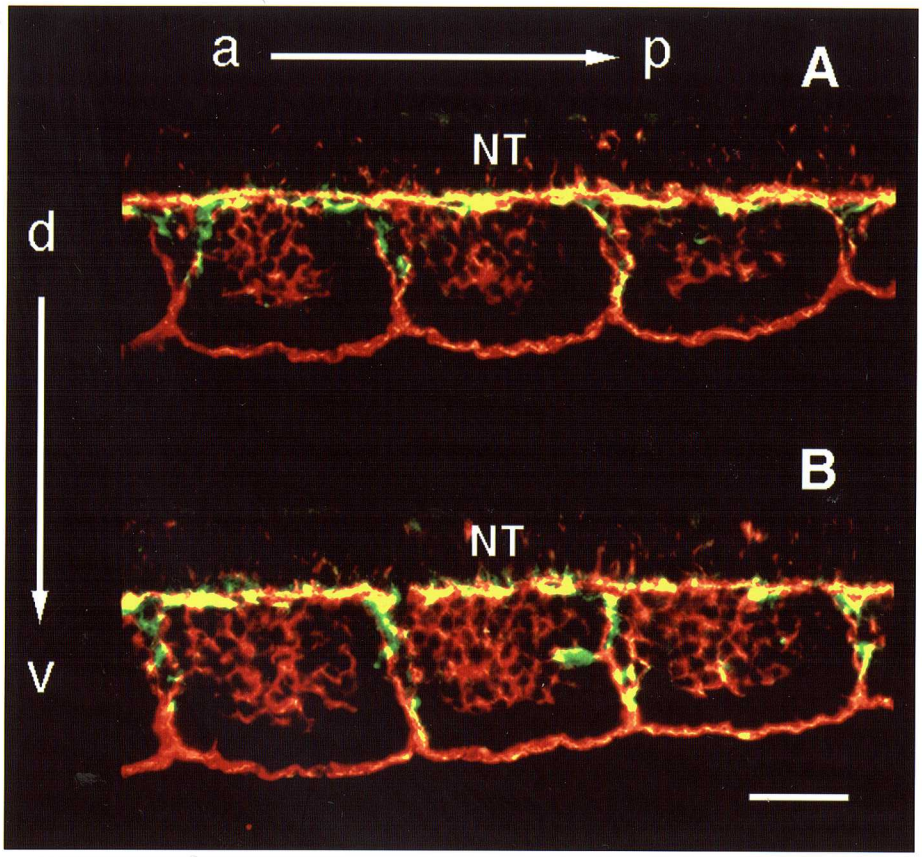

Fig. 6. Horizontal sections of dorsal (**A**) and ventral (**B**) portions at 16-18 somitic levels of 24-somite ddY embryo. Sections were double-stained with 4E9R and anti-chondroitin sulfate (CS-56). 4E9R-positive neural crest cells are not observed in sclerotomes. Note that chondroitin sulfate (red) is less present in the caudal portion of each sclerotome. a, anterior; p, posterior; d, dorsal; v, ventral; NT, neural tube. Bar: 50 μm.

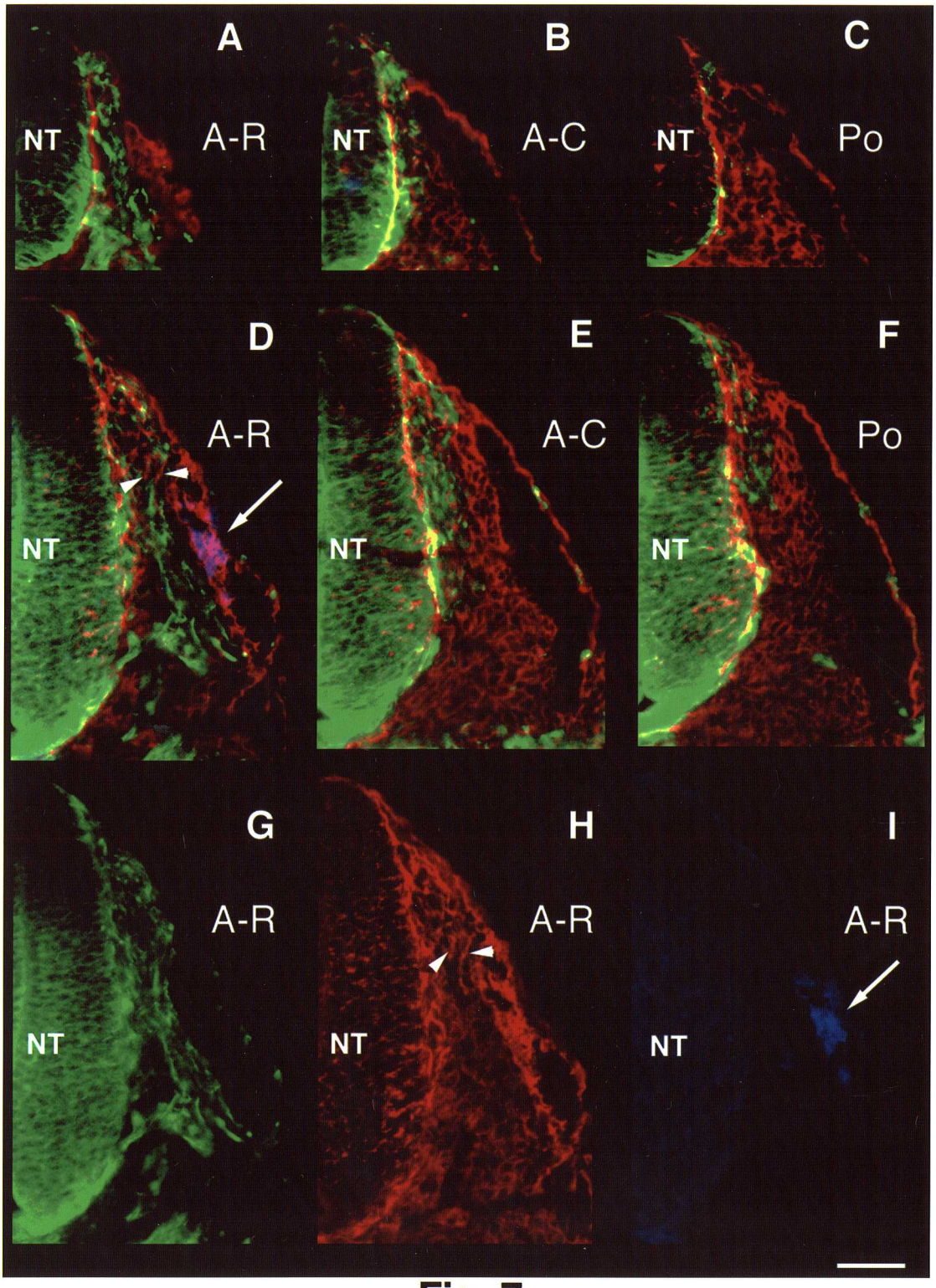

Fig. 7

Fig. 7. 4E9R-positive neural crest cells (green), chondroitin sulfate (CS; red) and tenascin (TN; blue) in sections triple-stained. (**A** - **C**) Transverse sections of A-R (**A**), A-C (**B**) and Po (**C**) regions at the 8 somitic level of 24-somite ddY embryo. Note that CS is not distributed in A-R (**A**). TN is not found at this stage. (**D** - **I**) Transverse sections of A-R (**D**, **G**, **H**, **I**), A-C (**E**) and Po (**F**) regions at the 8 somitic level of 28-somite ddY embryo. **G**, **H** and **I** show distributions of neural crest cells, CS and TN in the same A-R region as **D**, respectively. CS begins to be found in the dorsal portion of A-R region (arrowheads in **D** and **H**). TN is observed in the boundaries between adjacent dermamyotomes and between the dermamyotome and the sclerotome in A-R region (arrows in **D** and **I**). NT, neural tube. Bar: 50 μm.

root ganglionic region within A-C region and CS was absent in the presumptive ganglion (Fig. 7E). These changes of distribution patterns of CS in sclerotomes were similar at both forelimb-bud and hindlimb-bud levels. The distribution of TN was more spatiotemporally restricted. The immunoreactivities against TN in sclerotomes were only observed in A-R regions of late migratory stages at both forelimb-bud and hindlimb-bud levels (Fig. 7D-F, I). TN was localized in ventral portions of boundaries containing LN between adjacent dermamyotomes and between sclerotomes and dermamyotomes (Fig. 7D, Fig. 9D, G).

Migration patterns of neural crest cells in tenascin-knockout mouse embryos

To analyze the roles of TN in formation of migration patterns of neural crest cells, three-dimensional image analyses were performed in 28 somite stages at forelimb-bud levels, using TN-knockout mutant mice (C3H/HeN-TN$^-$/TN$^-$). A-R, A-C and Po were present in the mutant and the wild-type (C3H/HeN-TN$^+$/TN$^+$) sclerotome (Fig. 8A, Fig. 9A-C, Fig. 10A-C) and their sizes were similar in TN-knockout and wild-type mice (Fig. 8A). Semiquantitative estimates of the number of neural crest cells in ventrolateral pathways revealed that the number of these cells in TN-knockout embryos was smaller than that of the wild-type particularly in VP areas (Fig. 8B). TN was only present in ventral portions of anti-LN-positive boundaries between adjacent dermamyotomes in wild-type embryos and between sclerotomes and dermamyotomes in their A-R (Fig. 9D-H) and, on the other hand, no TN was seen in TN-knockout embryos (Fig. 10D, E). Sclerotomal distributions of CS in TN-knockout embryos (Fig. 10D, F) were similar to those in the wild-type (Fig. 9 G, I) or in ddY embryos.

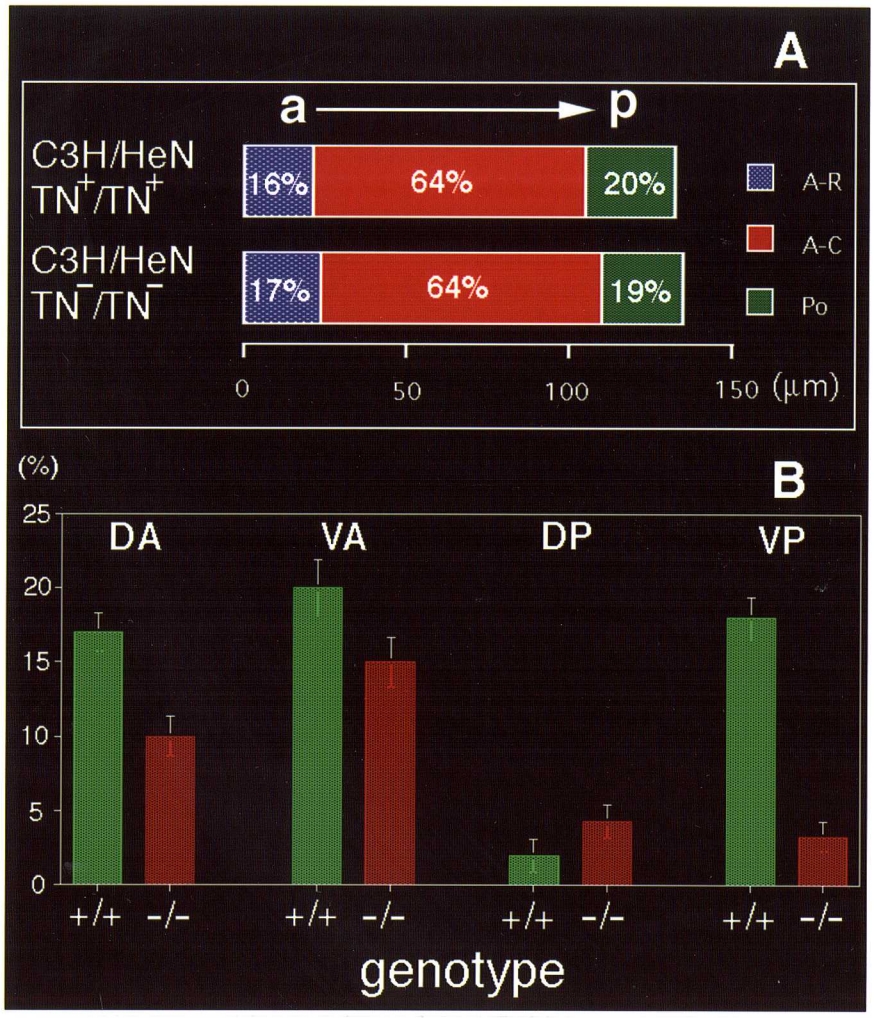

Fig. 8. Distribution patterns of neural crest cells at 8 somitic levels of 28-somite wild-type (C3H/HeN-TN^{+}/TN^{+}) and TN-knockout (C3H/HeN-TN^{-}/TN^{-}) embryos. (**A**) Percentage of the rostrocaudal length of A-R, A-C or Po region in the total sclerotome length. Measurements were performed using 3 or 4 embryos. (**B**) Semiquantitative analyses of the number of neural crest cells along ventrolateral pathways. Bars represent the mean of the counting performed in 2 or 4 embryos. Refer to Fig. 4 legend for abbreviations of DA, DP, VA and VP. a, anterior; p, posterior; +/+, wild-type mouse; -/-, TN-knockout mouse.

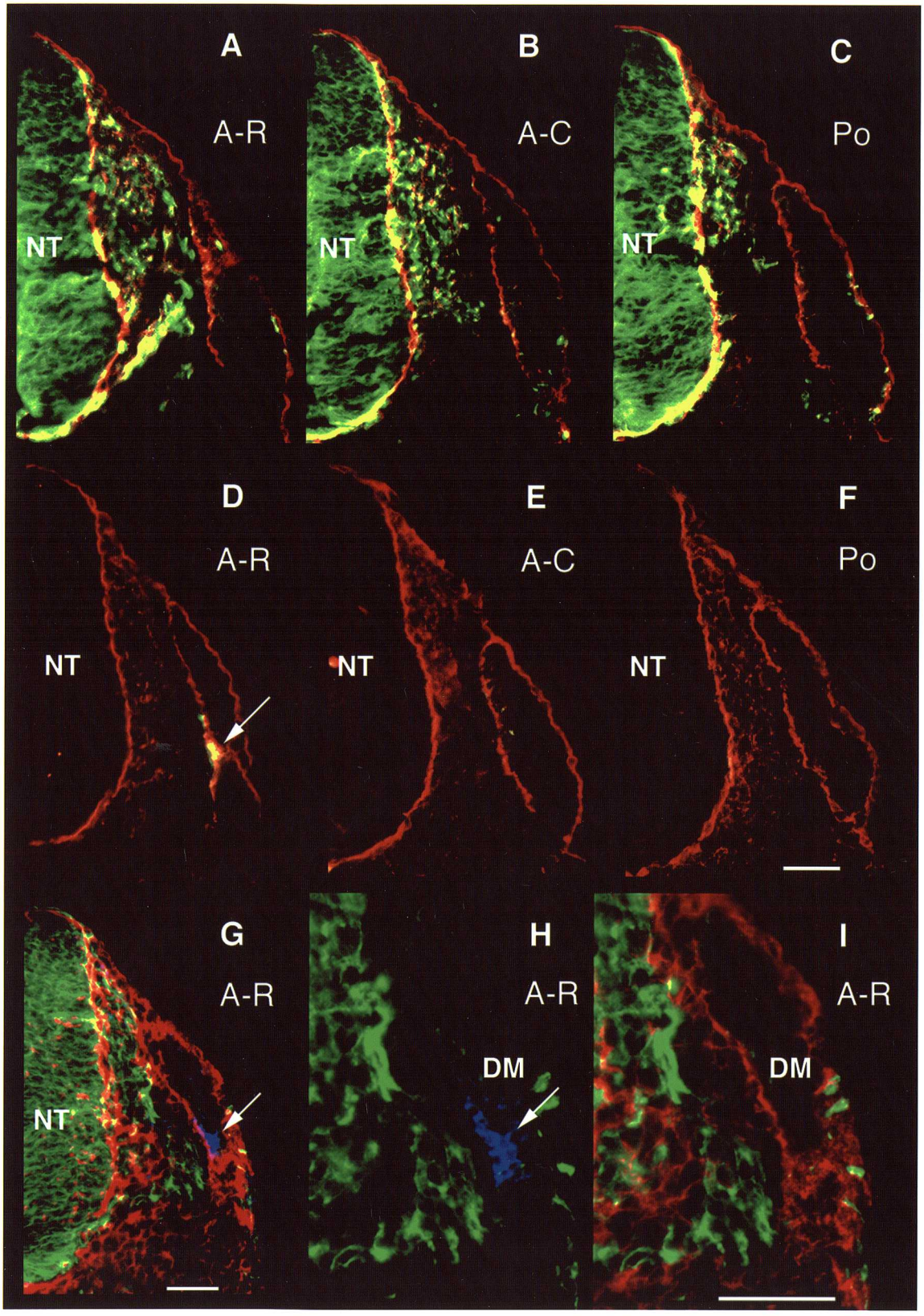

Fig. 9

Fig. 9. Transverse sections at 8 somitic levels of 28-somite wild-type embryos. (**A** - **C**) 4E9R-positive neural crest cells (green) and laminin (LN; red) in A-R (**A**), A-C (**B**) and Po (**C**) regions. A-R, A-C and Po regions are present in the sclerotome. (**D** - **F**) Transverse sections of A-R (**D**), A-C (**E**) and Po (**F**) regions. These sections were double-stained with monoclonal anti-tenascin and anti-LN. Tenascin (TN; arrow in **D**) is observed in the LN-containing boundary (red) between the dermamyotome and the sclerotome in A-R region. (**G**) Neural crest cells (green), chondoroitin sulfate (CS; red) and TN (blue; arrow) in A-R region. (**H**, **I**) Higher magnification of **G**. **H** and **I** show distributions of neural crest cells and TN (arrow in **H**) or CS (**I**). NT, neural tube; DM, dermamyotome. Bars, 50 μm.

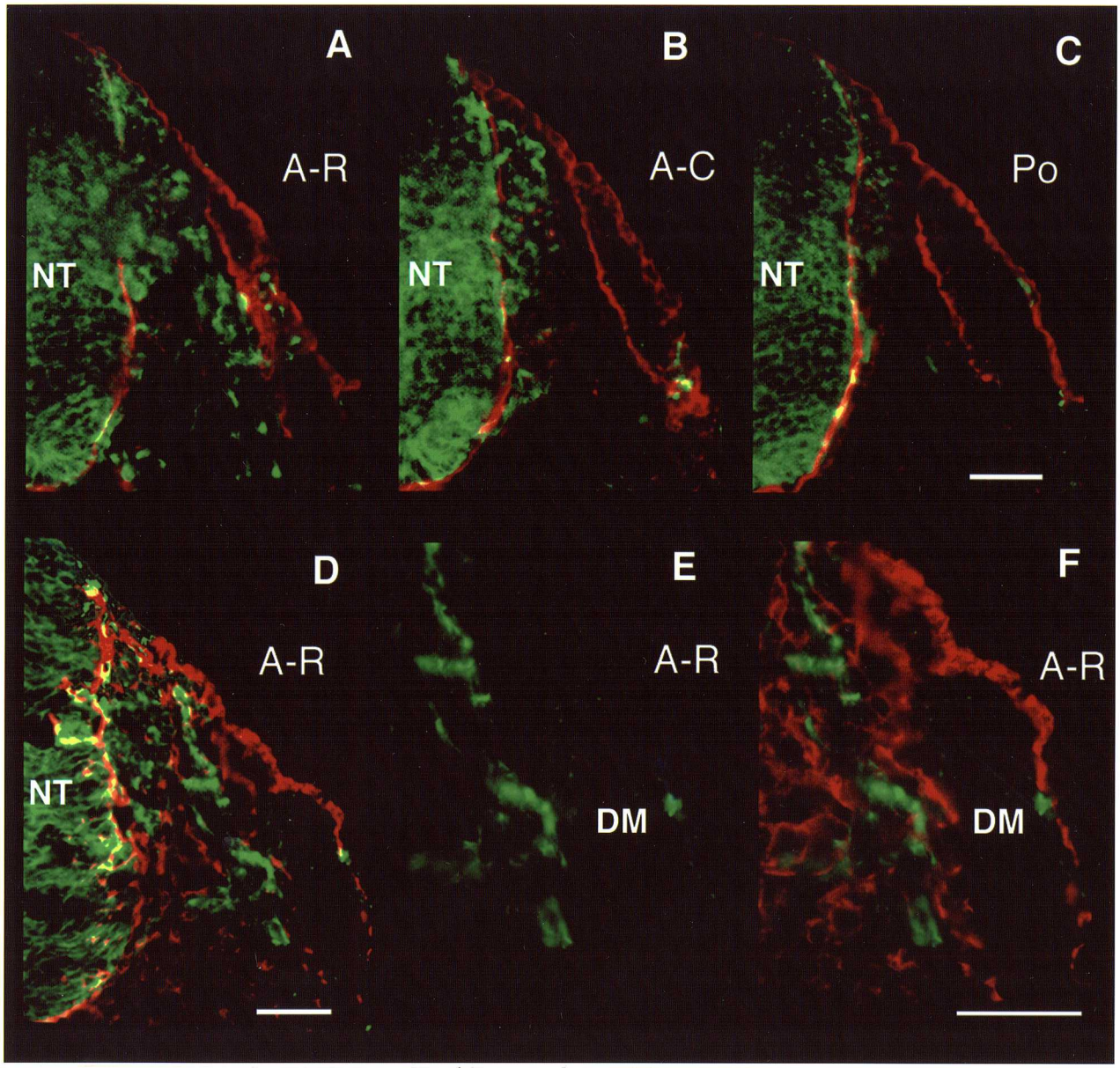

Fig. 10. Transverse sections at 8 somitic levels of 28-somite TN-knockout embryos. (**A - C**) 4E9R-positive neural crest cells (green) and laminin (red) in A-R (**A**), A-C (**B**) and Po (**C**) regions. Note that A-R, A-C and Po regions are found in the sclerotome. (**D**) Neural crest cells (green), chondroitin sulfate (CS; red) and tenascin (TN; blue) in A-R region. This section was triple-stained with 4E9R, anti-CS and anti-TN. (**E, F**) Higher magnification of **D**. **E** and **F** show distributions of neural crest cells and TN (**E**) or CS (**F**). TN is absent in TN-knockout embryos. NT, neural tube; DM, dermamyotome. Bars, 50 μm.

DISCUSSION

Migration patterns of trunk neural crest cells within the sclerotome

In the present study, we have shown that migration patterns of trunk neural crest cells in mouse embryos differ even in the rostral half of the sclerotome. At forelimb-bud levels (8 somitic levels), two regions having different migration patterns were found in the rostral half: A-R region where both ventrolateral and ventromedial pathways are present, and A-C region where the ventromedial route is only observed. The rostrocaudal extent of these regions changed during migratory stages of neural crest cells. The extent of A-R decreased along with the enlargement of A-C region, as their migratory stages advanced. Serbedzija et al. (1990) inferred that there were two overlapping migratory phases of mouse trunk neural crest cells at forelimb-bud levels: (1) early ventrolateral pathways which open by embryonic day (Ed) 9 and close by Ed 9.5, and (2) later ventromedial pathways which appear after Ed 9-9.5 and continue to be present through Ed 10.5. This well-founded conjecture has been assured by the present data. In this study, ventrolateral pathways were initially observed in 17 somite stages (Ed 9) at forelimb-bud levels. The number of neural crest cells migrating along the routes was rapidly reduced by Ed 9.5, that is at a period from 24 to 28 somite stages, accompanied with the decrease of A-R. Thus, this result reveals that the migration along ventrolateral pathways terminate by 28 somite stages (late stages of Ed 9.5). Ventromedial pathways in A-C regions continued to be present through 28 somite stages and the majority of neural crest cells in sclerotomes migrated along the ventromedial pathways after late stages of Ed 9.5. These data indicate that most of later emigrating crest cells move along ventromedial pathways.

We have observed that neural crest cells in A-R region extend ventrally to the level

of the sympathetic nerve plexus, migrating along the ventromedial pathway as well as the ventrolateral pathway. On the other hand, most of neural crest cells moving along the ventromedial pathway in A-C region ceased their migration at the level of the dorsal root ganglion. Since the portions in sclerotomes where neural crest cell migration occurs were occupied by A-R region in early migratory stages, most of early emigrating crest cells migrate in this region and might be populated in presumptive sympathetic chains. A later migrating group of cells moving along A-C might primarily colonize in the dorsal root ganglionic region. The similar pattern has been suggested in previous studies using mouse embryos (Serbedzija et al., 1990) and chick embryos (Weston and Butler, 1966; Serbedzija et al., 1989). At hindlimb-bud levels (23 somitic levels), temporal changes of the rostrocaudal extent of A-R and A-C regions were similar to those at forelimb-bud levels. It is possible that the underlying mechanisms to form migration patterns of neural crest cells are similar at both axial levels. However, the number of these cells migrating along ventrolateral pathways was smaller at hindlimb-bud levels than at forelimb-bud levels. At hindlimb-bud levels, furthermore, the number of neural crest cells in ventrolateral routes already reached maximum in early migratory stages (31 somite stages) in dorsal areas of these pathways (DA and DP). These results suggest that ventrolateral pathways may close earlier at hindlimb-bud levels and the proportion of neural crest cells migrating along the pathways may be smaller compared with forelimb-bud levels.

It has been shown in studies using chick embryos (Loring and Erickson, 1987; Tosney et al., 1994) that anti-laminin-positive basal lamina on the boundary between the dermamyotome and the sclerotome plays an important role in formation of the ventrolateral pathway. In the mouse, however, basal lamina containing laminin (LN) at the medial side of the dermamyotome were not found in early migratory stages of neural crest cells when ventrolateral pathways appears (Fig. 11). A similar staining pattern can be seen in the previous study using mouse embryos (Sternberg and Kimber, 1986a).

Moreover, ventrolateral routes continued to be absent in A-C regions even when the anti-LN-positive basal lamina was apparent. These results suggest that dermamyotomal anti-LN-positive basal lamina over the sclerotome may not be necessarily required to form the ventrolateral pathway in the mouse embryo. At forelimb-bud levels, the increase of neural crest cells in ventrolateral pathways was related to the initial appearance of the basal lamina containing LN (Fig. 11). It is conceivable that the basal lamina may facilitate neural crest cell migration along the ventrolateral pathway.

Chondroitin sulfate is essential for pattern formation of trunk neural crest cell migration

In double- and triple-stainings using 4E9R and anti-extracellular matrix molecules, we found characteristic patterns of distributions of chondroitin sulfate (CS) related to migration patterns of mouse trunk neural crest cells. As mentioned in studies using rat and mouse embryos performed by Morriss-Kay and her colleagues (Morriss-Kay and Tuckett, 1989; Trasler and Morriss-Kay, 1991), most mesenchymal cells including neural crest cells are stained by anti-CS (CS-56) when CS-56 is used in staining conditions of the low dilution and/or the long incubation. Under the condition used in this study, however, immunoreactivities of neural crest cells to CS-56 disappeared and the staining intensity within the sclerotome spatiotemporally changed. Thus, staining patterns of CS-56 observed in this study represent distribution patterns of CS within the sclerotome. As summarized in Fig. 11, distributions of CS temporally changed: (1) before the invasion of neural crest cells into the sclerotome (premigratory stage in Fig. 11), CS-rich regions shifted from the core of the somite to the anterior portion of the sclerotome. (2) In early to middle migratory stages of neural crest cells, CS-deposition appeared to follow a caudal-to-rostral sequence within the sclerotome. (3) In their late migratory stages, CS began to be distributed in the dorsal portion of A-R region. These observations show

that CS is abundant in regions where neural crest cells are absent. Thus, dynamic distributions of CS are closely related to systematic changes of migration of mouse trunk neural crest cells observed in this study (Fig. 11). Distribution patterns of CS described above are similar to those of chondroitin sulfate proteoglycans (CS-PG) shown in the study using chick embryos (Perris et al., 1991). It has been suggested that CS-PG act as barriers to neural crest cell migration and axon outgrowth of motor neurons in the chicken (Newgreen et al., 1990; Oakley and Tosney, 1991; Landolt et al., 1995). We could not use antibodies against core proteins of CS-PG. Types of CS-PG having the dynamic distributions observed in this study remain to be unknown. However, it is possible that proteoglycans containing CS may contribute to pattern formation of neural crest cell migration in the mouse trunk by means of their site-restricted distributions, their ability to modulate migration on other substrates such as fibronectin (Tan et al., 1987) which is uniformly distributed in sclerotomes.

The role of tenascin in pattern formation of trunk neural crest cell migration

Tenascin (TN) appeared in the part of the boundary containing LN between the dermamyotome and the sclerotome in A-R region, corresponding to the ventral portion of the ventrolateral pathway, after late migratory stages of mouse trunk neural crest cells (Fig. 11). A similar distribution of TN was observed in rat embryos (Mackie et al., 1988). Furthermore, migration patterns of trunk neural crest cells in TN-knockout embryos were comparable with those of wild-type crest cells. These results support the conclusion that TN is not directly responsible for the segmented outgrowth of trunk neural crest cells (Stern et al., 1989; Newgreen et al., 1990). However, the number of neural crest cells in ventroposterior areas of ventrolateral pathways (VP), where TN was distributed in wild-type embryos, was significantly reduced in TN-knockout mice. It is conceivable that TN may act as a modulatory factor in termination of neural crest cell migration along

ventrolateral pathways, perhaps by modifying the interaction of neural crest cells with other extracellular matrices (Mackie et al., 1988; Halfter et al., 1989).

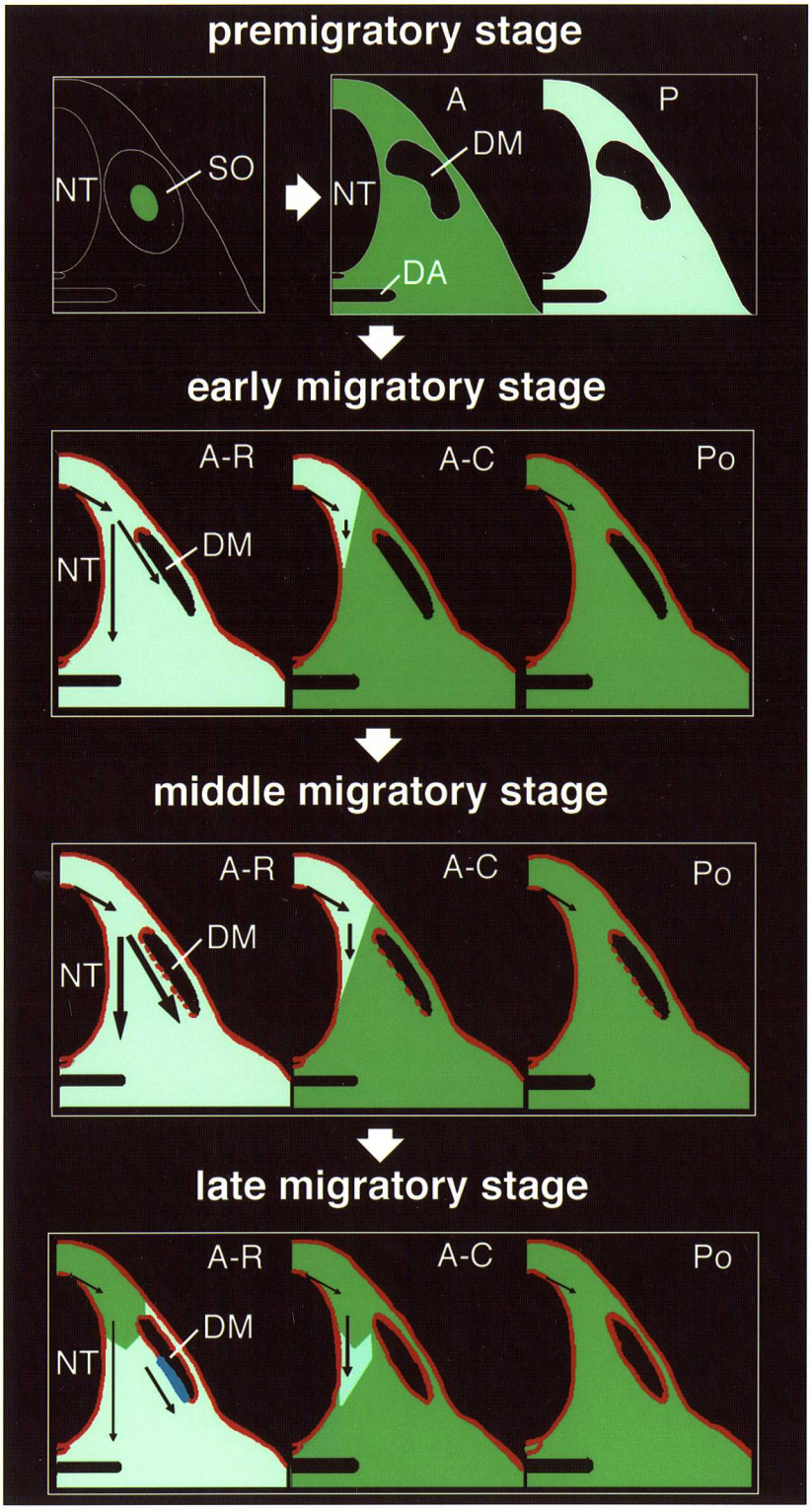
premigratory stage
NT
SO
A
P
DM
NT
DA
early migratory stage
A-R
A-C
Po
DM
NT
middle migratory stage
A-R
A-C
Po
DM
NT
late migratory stage
A-R
A-C
Po
DM
NT

Fig. 11

Fig. 11. Schematic diagram of migration patterns of trunk neural crest cells and distribution patterns of extracellular matrix molecules in mouse embryos. See DISCUSSION in the text for a detailed explanation of this figure. premigratory stage, stage before the invasion of neural crest cells into sclerotomes; early migratory stage, 17 somite stage at forelimb-bud level or 31 somite stage at hindlimb-bud level; middle migratory stage, 24 somite stage at forelimb-bud level or 37 somite stage at hindlimb-bud level; late migratory stage, 28 somite stage at forelimb-bud level or 39 somite stage at hindlimb-bud level. red, anti-laminin-positive basal lamina; blue, anti-tenascin-positive region; green, chondroitin-sulfate (CS)-rich region; light green, CS-poor region. NT, neural tube; SO, somite; DA, dorsal aorta; DM, dermamyotome.

CONCLUSION

1. The neural crest is an unique tissue in the vertebrate embryo and play an important role in construction of the vertebrate body organization. Laboratory mice are particularly useful for genetic studies of migration and differentiation of neural crest cells. However, little has been known about development of mouse neural crest cells. We therefore produced a rat anti-mouse monoclonal antibody (4E9R) which identifies mouse neural crest cells to analyze migration patterns of these cells. Distributions of 4E9R-immunoreactive cells in mouse embryos have shown that this antibody recognizes cranial and trunk neural crest cells before their expression of overt differentiation phenotypes.

2. It has been shown in cultures treated with colchicine or cytochalasin B that 4E9R antigens are present in intermediate filaments. When three-dimensional image analyses using a confocal laser scanning microscope and image-analyzing software were performed to analyze distributions of 4E9R-antigens in mouse neural crest cells, furthermore, their distributions were similar to those of vimentin which is a typical intermediate filament in most mesenchymal cells including neural crest cells. However, distributions of 4E9R-positive cells and anti-vimentin-immunoreactive cells differed in mouse embryos. These results have suggested that 4E9R-antigens are vimentin-related and specifically expressed in restricted types of cells including mouse neural crest cells.

3. We have examined migration patterns of mouse neural crest cells in the sclerotome by means of the three-dimensional image analysis. Three types of regions (A-R, A-C and Po regions) within each sclerotome, among which migration patterns of

neural crest cells differed, were found along the anteroposterior axis. At the rostral level of the anterior half of the sclerotome, both ventromedial and ventrolateral pathways were observed (A-R region). The region, where the ventromedial rote was only present (A-C region), caudally followed A-R region. No neural crest cells were seen in the posterior half of the sclerotome (Po region).

4. The rostrocaudal extent of A-R, A-C and Po regions changed during migratory stages of neural crest cells. The extent of A-R region decreased along with the enlargement of A-C, as their migratory stages advanced. Since these alterations of A-R and A-C sizes suggested changes of the number of neural crest cells in ventrolateral pathways, these cells in the routes were semiquantitatively counted. It has been indicated that the reduction of the number of neural crest cells migrating along ventrolateral pathways is related to the alterations of A-R and A-C sizes along the anteroposterior axis.

5. In order to elucidate the roles of extracellular matrix molecules in formation of migration patterns of mouse neural crest cells in the trunk, double- and triple-stainings with 4E9R and anti-extracellular matrix molecules were performed. Distribution patterns of chondroitin sulfate were complementary to migration patterns of neural crest cells in the sclerotome. We conclude that spatiotemporally systematic changes of distributions of chondroitin sulfate in the sclerotome are one of indispensable requisites for formation of the migration patterns.

6. It has been controversial that how tenascin (TN) participates in migration of neural crest cells. In this study, TN appeared in the sclerotome after late migratory stages of neural crest cells. Migration patterns of these cells in TN-knockout mouse embryos were comparable with those of wild-type crest cells. These results

support the conclusion that TN is not directly responsible for the segmented outgrowth of trunk neural crest cells. However, the number of neural crest cells migrating along ventrolateral pathways was significantly reduced in TN-knockout embryos. It is conceivable that TN may act as a modulatory factor in termination of neural crest cell migration along ventrolateral pathways.

ACKNOWLEDGMENTS

I wish to express my gratitude to Prof. Toshiteru Morita and Dr. Kazuo Ito for many valuable suggestions and for continuous encouragements during the course of this work. I thank Dr. Moriaki Kusakabe of Division of Experimental Animal Research, RIKEN for kindly providing tenascin-knockout mice and monoclonal antibodies against tenascin. Polyclonal anti-tenascin antibodies were kindly supplied by Prof. Teruyo Sakakura of Mie University. I also thank Prof. Kazuhiko Tsuneki, Prof. Yasuo Nakanishi, Dr. Shinri Horiuchi, Dr. Yohki Hieda and Dr. Hidetaka Furuya for their helpful advice.

REFERENCES

Avnur, Z. and Geiger, B. (1984) Immunocytochemical localization of native chondroitin-sulfate in tissues and cultured cells using specific monoclonal antibody. Cell **38**, 811-822.

Albers, K. and Fuchs, E. (1992) The molecular biology of intermediate filament proteins. Int. Rev. Cytology **134**, 243-279.

Baynash, A. G., Hosoda, K., Giaid, A., Richardson, J. A., Emoto, N., Hammer, R. E. and Yanagisawa, M. (1994) Interaction of endothelin-3 with endothelin-B receptor is essential for development of epidermal melanocytes and enteric neurons. Cell **79**, 1277-1285.

Boyer, B., Tucker, G. C., Vallés, A. M., Franke, W. W. and Thiery, J. P. (1989) Rearrangements of desmosomal and cytoskeletal proteins during the transition from epithelial to fibroblastoid organization in cultured rat bladder carcinoma cells. J. Cell Biol. **109**, 1495-1509.

Bronner-Fraser, M. (1986) Analysis of the early stages of trunk neural crest migration in avian embryos using monoclonal antibody HNK-1. Dev. Biol. **115**, 44-55.

Bronner-Fraser, M. (1993) Environmental influences on neural crest cell migration. J. Neurobiol. **24**, 233-247.

Chan, W. Y. and Tam, P. P. L. (1988) A morphological and experimental study of the mesencephalic neural crest cells in the mouse embryo using wheat germ agglutinin-gold conjugate as the cell marker. Development **102**, 427-442.

Chiquet-Ehrismann, R., Mackie, E. J., Pearson, C. A. and Sakakura, T. (1986) Tenascin: an extracellular matrix protein involved in tissue interactions during fetal development and oncogenesis. Cell **47**, 131-139.

Chou, Y-H., Bischoff, J. R., Beach, D. and Goldman, R. D. (1990) Intermediate filament reorganization during mitosis is mediated by $p34^{cdc2}$ phosphorylation of vimentin. Cell **62**, 1063-1071.

Ciment, G., Ressler, A, Letourneau, P. C. and Weston, J. A. (1986) A novel intermediate filament-associated protein, NAPA-73, that binds to different filament types at different stages of nervous system development. J. Cell Biol. **102**, 246-251.

Cochard, P. and Paulin, D. (1984) Initial expression of neurofilaments and vimentin in the central and peripheral nervous system of the mouse embryo in vivo. J. Neurosci. **4**, 2080-2094.

Coffin, J. D. and Poole, T. J. (1988) Embryonic vascular development: immunohistochemical identification of the origin and subsequent morphogenesis of the major vessel primordia in quail embryos. Development **102**, 735-748.

Erickson, C. A., Loring, J. F. and Lester, S. M. (1989) Migratory pathways of HNK-1-immunoreactive neural crest cells in the rat embryo. Dev. Biol. **134**, 112-118.

Erickson, C. A., Tucker, R. P. and Edwards, B. F. (1987) Changes in the distribution of intermediate-filament types in Japanese quail embryos during morphogenesis. Differentiation **34**, 88-97.

Erickson, C. A. and Weston, J. A. (1983) An SEM analysis of neural crest migration in the mouse. J. Embryol. exp. Morph. **74**, 97-118.

Franke, W. W., Grund, C., Kuhn, C., Jackson, B. W. and Illmensee, K. (1982) Formation of cytoskeletal elements during mouse embryogenesis III. Primary mesenchymal cells and the first appearance of vimentin filaments. Differentiation **23**, 43-59.

Garcia-Martinez, V. and Schoenwolf, G. C. (1993) Primitive-streak origin of the cardiovascular system in avian embryos. Dev. Biol. **159**, 706-719.

George, E. L., Georges-Labouesse, E. N., Patel-King, R. S., Rayburn, H. and Hynes, R. O. (1993) Defects in mesoderm, neural tube and vascular development in mouse embryos lacking fibronectin. Development **119**, 1079-1091.

Greenburg, G. and Hay, E. D. (1988) Cytoskeleton and thyroglobulin expression change during transformation of thyroid epithelium to mesenchyme-like cells. Development **102**, 605-622.

Guillemot, F., Lo, L-C., Johnson, J. E., Auerbach, A., Anderson, D. J. and Joyner, A. L. (1993) Mammalian achaete-scute homolog 1 is required for the early development of olfactory and autonomic neurons. Cell **75**, 463-476.

Halfter, W., Chiquet-Ehrismann, R. and Tucker, R. P. (1989) The effect of tenascin and embryonic basal lamina on the behavior and morphology of neural crest cells in vitro. Dev. Biol. **132**, 14-25.

Hall, B. K. (1988) " The Neural Crest", London, New York, Tokyo, Tronto: Oxford University Press.

Hasegawa, K., Yoshida, T., Matsumoto, K., Katsuta, K., Waga, S. and Sakakura, T. Differential expression of tenascin-c and tenascin-x in human astrocytomas. Acta Neuropathol. in press.

Hosoda, K., Hammer, R. E., Richardson, J. A., Baynash, A. G., Cheung, J. C., Giaid, A. and Yanagisawa, M. (1994) Targeted and natural (Piebald-Lethal) mutations of endothelin-B receptor gene produce megacolon associated with spotted coat color in mice. Cell **79**, 1267-1276.

Hou, L. and Takeuchi, T. (1994) Neural crest development in reptilian embryos, studied with monoclonal antibody, HNK-1. Zool. Sci. **11**, 423-431.

Hunt, P., Whiting., J., Muchamore, I., Marshall, H. and Krumlauf, R. (1991) Homeobox genes and models for patterning the hindbrain and branchial arches. Development Supplement **1**, 187-196.

Ito, K. and Takeuchi, T. (1984) The differentiation in vitro of the neural crest cells of the mouse embryos. J. Embryol. exp. Morph. **84**, 49-62.

Ito, K. and Sieber-Blum, M. (1991) In vitro clonal analysis of quail cardiac neural crest development. Dev. Biol. **148**, 95-106.

Ito, K., Morita, T. and Sieber-Blum, M. (1993) In vitro clonal analysis of mouse neural crest development. Dev. Biol. **157**, 517-525.

Keynes, R. J. and Stern, C. D. (1984) Segmentation in the vertebrate nervous system. Nature **310**, 786-789.

Keynes, R. J. and Stern, C. D. (1988) Mechanisms of vertebrate segmentation. Development **103**, 413-429.

Koyama, Y., Norose, K., Kusubata, M., Irie S. and Kusakabe, M. (1996) Differential expression of tenascin in the skin during hapten-induced dermatitis. Histochem. Cell Biol. **106**, 263-273.

Kubota, Y., Morita, T. and Ito K. (1996) New monoclonal antibody (4E9R) identifies mouse neural crest cells. Dev. Dyn. **206**, 368-378.

Landolt, R. M., Vaughan, L., Winterhalter, K. H. and Zimmermann, D. R. (1995) Versican is selectively expressed in embryonic tissues that act as barriers to neural crest migration and axon outgrowth. Development **121**, 2303-2312.

Le Douarin, N. (1973) A biological cell labeling technique and its use in experimental embryology. Dev. Biol. **30**, 217-222.

Le Douarin, N. M. (1982) "The neural crest.", Cambridge, U. K.: Cambridge University Press.

Lendahl, U., Zimmerman, L. B. and McKay, R. D. G. (1990) CNS stem cells express a new class of intermediate filament protein. Cell **60**, 585-595.

Loring, J. F. and Erickson, C. A. (1987) Neural crest cell migratory pathways in the trunk of the chick embryo. Dev. Biol. **121**, 220-236.

Mackie, E. J., Tucker, R. P., Halfter, W., Chiquet-Ehrismann, R. and Epperlein, H. H. (1988) The distribution of tenascin coincides with pathways of neural crest cell migration. Development **102**, 237-250.

Martins-Green, M. and Erickson, C. A. (1986) Development of neural tube basal lamina during neurulation and neural crest cell emigration in the trunk of the mouse embryo. J. Embryol. exp. Morph. **98**, 219-236.

Morrison-Graham, K. and Weston, J. A. (1989) Mouse mutants provide new insights into the role of extracellular matrix in cell migration and differentiation. Trends Genet. **5**, 116-121.

Morriss-Kay, G. and Tuckett, F. (1989) Immunohistochemical localisation of chondroitin sulphate proteoglycans and the effects of chondroitinase ABC in 9- to 11-day rat embryos. Development **106**, 787-798.

Newgreen, D. F., Powell, M. E. and Moser, B. (1990) Spatiotemporal changes in HNK-1/L2 glycoconjugates on avian embryo somite and neural crest cells. Dev. Biol. **139**, 100-120.

Nichols, D. H. (1981) Neural crest formation in the head of the mouse embryo as observed using a new histological technique. J. Embryol. exp. Morph. **64**, 105-120.

Nichols, D. H. (1986) Formation and distribution of neural crest mesenchyme to the first pharyngeal arch region of the mouse embryo. Am. J. Anat. **176**, 221-231.

Oakley, R. A. and Tosney, K. W. (1991) Peanut agglutinin and chondroitin-6-sulfate are molecular markers for tissues that act as barriers to axon advance in the avian embryo. Dev. Biol. **147**, 187-206.

Osumi-Yamashita, N., Ninomiya, Y., Doi, H. and Eto, K. (1994) The contribution of both forebrain and midbrain crest cells to the mesenchyme in the frontonasal mass of mouse embryos. Dev. Biol. **164**, 409-419.

Pardanaud, L., Altmann, C., Kitos, P., Dieterlen-Lievre, F. and Buck, C. A. (1987) Vasculogenesis in the early quail blastodisc as studied with a monoclonal antibody recognizing endothelial cells. Development **100**, 339-349.

Perris, R., Krotoski, D., Lallier, T., Domingo, C., Sorrell, J. M. and Bronner-Fraser, M. (1991) Spatial and temporal changes in the distribution of proteoglycans during avian neural crest development. Development **111**, 583-599.

Rickmann, M., Fawcett, J. W. and Keynes, R. J. (1985) The migration of neural crest cells and the growth of motor axons through the rostral half of the chick somite. J. Embryol. exp. Morph. **90**, 437-455.

Sadaghiani, B. and Vielkind, J. R. (1990) Distribution and migration pathways of HNK-1-immunoreactive neural crest cells in teleost fish embryos. Development **110**, 197-209.

Saga, Y., Yagi, T., Ikawa, Y., Sakakura, T. and Aizawa, S. (1992) Mice develop normally without tenascin. Genes Dev. **6**, 1821-1831.

Schuchardt, A., D'Agati, V., Larsson-Blomberg, L., Costantini, F. and Pachnis, V. (1994) Defects in the kidney and enteric nervous system of mice lacking the tyrosine kinase receptor Ret. Nature **367**, 380-383.

Serbedzija, G. N., Bronner-Fraser, M. and Fraser, S. E. (1989). A vital dye analysis of the timing and pathways of avian trunk neural crest cell migration. Development **106**, 809-816.

Serbedzija, G. N., Bronner-Fraser, M. and Fraser, S. E. (1992) Vital dye analysis of cranial neural crest cell migration in the mouse embryo. Development **116**, 297-307.

Serbedzija, G. N., Fraser, S. E. and Bronner-Fraser, M. (1990) Pathways of trunk neural crest cell migration in the mouse embryo as revealed by vital dye labelling. Development **108**, 605-612.

Silvers, W. K. (1979) "The coat colors of mice", New York, Heidelberg, Berlin: Springer-verlag.

Steinert, P. M. and Roop, D. R. (1988) Molecular and cellular biology of intermediate filaments. Ann. Rev. Biochem. **57**, 593-625.

Stern, C. D., Norris, W. E., Bronner-Fraser, M., Carlson, G. J., Faissner, A., Keynes, R. J. and Schachner, M. (1989) J1/tenascin-related molecules are not responsible for the segmented pattern of neural crest cells or motor axons in the chick embryo. Development **107**, 309-319.

Sternberg, J. and Kimber, S. J. (1986a) Distribution of fibronectin, laminin and entactin in the environment of migrating neural crest cells in early mouse embryos. J. Embryol. exp. Morph. **91**, 267-282.

Sternberg, J. and Kimber, S. J. (1986b) The relationship between emerging neural crest cells and basement membranes in the trunk of the mouse embryo: a TEM and immunocytochemical study. J. Embryol. exp. Morph. **98**, 251-268.

Tan, S-S., Crossin, K. L., Hoffman, S. and Edelman, G. M. (1987) Asymmetric expression in somites of cytotactin and its proteoglycan ligand is correlated with neural crest cell distribution. Proc. Natl. Acad. Sci. USA **84**, 7977-7981.

Tan, S. S. and Morriss-Kay, G. M. (1986) Analysis of cranial neural crest cell migration and early fates in postimplantation rat chimaeras. J. Embryol. exp. Morph. **98**, 21-58.

Tan, S-S., Prieto, A. L., Newgreen, D. F., Crossin K. L. and Edelman, G. M. (1991) Cytotactin expression in somites after dorsal neural tube and neural crest ablation in chicken embryos. Proc. Natl. Acad. Sci. USA **88**, 6398-6402.

Tanaka, S., Yamamoto, H., Takeuchi, S. and Takeuchi, T. (1990) Melanization in albino mice transformed by introducing cloned mouse *tyrosinase* gene. Development **108**, 223-227.

Tosney, K. W., Dehnbostel, D. B. and Erickson, C. A. (1994) Neural crest cells prefer the myotome's basal lamina over the sclerotome as a substratum. Dev. Biol. **163**, 389-406.

Trasler, D. G. and Morriss-Kay, G. (1991) Immunohistochemical localization of chondroitin and heparan sulfate proteoglycans in pre-spina bifida splotch mouse embryos. Teratology **44**, 571-579.

Tucker, G. C., Aoyama, H., Lipinski, M., Tursz, T. and Thiery, J. P. (1984) Identical reactivity of monoclonal antibodies HNK-1 and NC-1: conservation in vertebrates on cells derived from the neural primordium and on some leukocytes. Cell Differ. **14**, 223-230.

Vidrich, A., Gilmartin, M., Zimmerman, J. and Freedberg, I. M. (1982) Glycosylation of the keratin intermediate filaments of ME-180. J. Cell Biol. **96(2, Pt. 2)**, 237a.

Vincent, M. and Thiery, J-P. (1984) A cell surface marker for neural crest and placodal cells: Further evolution in peripheral and central nervous system. Dev. Biol. **103**, 468-481.

Weston, J. A. (1963) A radioautographic analysis of the migration and localization of trunk neural crest cells in the chick. Dev. Biol. **6**, 279-310.

Weston, J. A. (1970) The migration and differentiation of neural crest cells. Adv. Morphogen. **8**, 41-114.

Weston, J. A. and Butler, S. L. (1966) Temporal factors affecting localization of neural crest cells in the chicken embryo. Dev. Biol. **14**, 246-266.

Ziller, C., Dupin, E., Brazeau, P., Paulin, D. and Le Douarin, N. M. (1983) Early segregation of a neuronal precursor cell line in the neural crest as revealed by culture in a chemically defined medium. Cell **32**, 627-638.